Cell Reports
Medicine

Article

Dynamics of AMPA receptors regulate epileptogenesis in patients with epilepsy

Graphical abstract

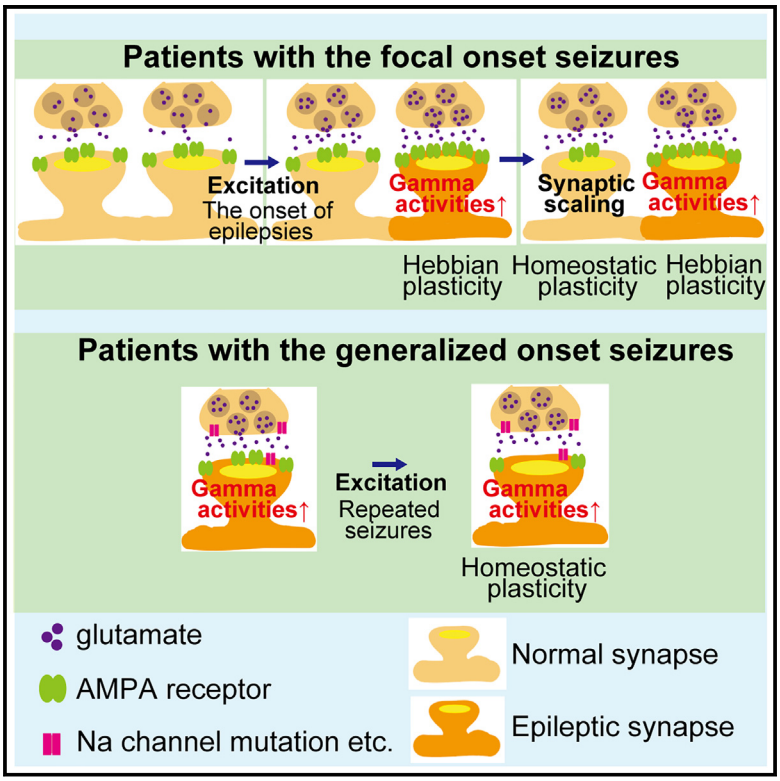

Highlights

- We quantify levels of AMPARs in epilepsy patients and controls using PET tracer [^{11}C]K-2
- Increased AMPARs augment the amplitude of abnormal gamma activity
- Cell-surface AMPARs are generally decreased in patients with epilepsy
- Hebbian plasticity and homeostatic scaling regulate epileptic brain function

Authors

Tsuyoshi Eiro, Tomoyuki Miyazaki, Mai Hatano, ..., Riki Matsumoto, Akio Ikeda, Takuya Takahashi

Correspondence

takahast@yokohama-cu.ac.jp

In brief

Eiro et al. measure the density of cell-surface AMPARs in 30 epilepsy patients and 31 healthy controls with the PET tracer [^{11}C]K-2. Increased cell surface AMPARs augment abnormal gamma activity, while patients with epilepsy generally exhibit reduced cell-surface AMPARs. Thus, Hebbian and homeostatic plasticity regulate epileptic brain function.

Eiro et al., 2023, Cell Reports Medicine *4*, 101020
May 16, 2023
https://doi.org/10.1016/j.xcrm.2023.101020

CellPress

Cell Reports Medicine

CellPress
OPEN ACCESS

Article

Dynamics of AMPA receptors regulate epileptogenesis in patients with epilepsy

Tsuyoshi Eiro,[1,5,16] Tomoyuki Miyazaki,[1,16] Mai Hatano,[1] Waki Nakajima,[1] Tetsu Arisawa,[1] Yuuki Takada,[1] Kimito Kimura,[1] Akane Sano,[1] Kotaro Nakano,[1] Takahiro Mihara,[2] Yutaro Takayama,[3] Naoki Ikegaya,[3] Masaki Iwasaki,[4] Akitoyo Hishimoto,[5] Yoshihiro Noda,[6] Takahiro Miyazaki,[6] Hiroyuki Uchida,[6] Hideaki Tani,[6] Nobuhiro Nagai,[6] Teruki Koizumi,[6] Shinichiro Nakajima,[6] Masaru Mimura,[6] Nozomu Matsuda,[7] Kazuaki Kanai,[7] Kazuhiro Takahashi,[8] Hiroshi Ito,[8,9] Yoji Hirano,[10,11] Yuichi Kimura,[12] Riki Matsumoto,[13] Akio Ikeda,[14] and Takuya Takahashi[1,15,17,*]

[1]Department of Physiology, Yokohama City University Graduate School of Medicine, Yokohama 236-0004, Japan
[2]Department of Health Data Science, Yokohama City University Graduate School of Data Science, Yokohama 236-0004, Japan
[3]Department of Neurosurgery, Yokohama City University Graduate School of Medicine, Yokohama 236-0004, Japan
[4]Department of Neurosurgery, National Center Hospital, National Center of Neurology and Psychiatry, Kodaira 187-8551, Japan
[5]Department of Psychiatry, Yokohama City University Graduate School of Medicine, Yokohama 236-0004, Japan
[6]Department of Neuropsychiatry, Keio University School of Medicine, Tokyo 160-0016, Japan
[7]Department of Neurology, Fukushima Medical University, Fukushima 960-1295, Japan
[8]Advanced Clinical Research Center, Fukushima Global Medical Science Center, Fukushima Medical University, Fukushima 960-1295, Japan
[9]Department of Radiology and Nuclear Medicine, Fukushima Medical University, Fukushima 960-1295, Japan
[10]Department of Neuropsychiatry, Graduate School of Medical Sciences, Kyushu University, Fukuoka 812-8582, Japan
[11]Department of Psychiatry, Division of Clinical Neuroscience, Faculty of Medicine, University of Miyazaki, 5200 Kihara, Kiyotake, Miyazaki 889-1692, Japan
[12]Faculty of Informatics, Cyber Informatics Research Institute, Kindai University, Higashi-Osaka 577-8502, Japan
[13]Division of Neurology, Kobe University Graduate School of Medicine, Kobe 650-0017, Japan
[14]Department of Epilepsy, Movement Disorders and Physiology, Kyoto University Graduate School of Medicine, Kyoto 606-8507, Japan
[15]The University of Tokyo, International Research Center for Neurointelligence, Tokyo 113-0033, Japan
[16]These authors contributed equally
[17]Lead contact
*Correspondence: takahast@yokohama-cu.ac.jp
https://doi.org/10.1016/j.xcrm.2023.101020

SUMMARY

The excitatory glutamate α-amino-3-hydroxy-5-methyl-4-isoxazole propionic acid receptors (AMPARs) contribute to epileptogenesis. Thirty patients with epilepsy and 31 healthy controls are scanned using positron emission tomography with our recently developed radiotracer for AMPARs, [^{11}C]K-2, which measures the density of cell-surface AMPARs. In patients with focal-onset seizures, an increase in AMPAR trafficking augments the amplitude of abnormal gamma activity detected by electroencephalography. In contrast, patients with generalized-onset seizures exhibit a decrease in AMPARs coupled with increased amplitude of abnormal gamma activity. Patients with epilepsy had reduced AMPAR levels compared with healthy controls, and AMPARs are reduced in larger areas of the cortex in patients with generalized-onset seizures compared with those with focal-onset seizures. Thus, epileptic brain function can be regulated by the enhanced trafficking of AMPAR due to Hebbian plasticity with increased simultaneous neuronal firing and compensational downregulation of cell-surface AMPARs by the synaptic scaling.

INTRODUCTION

Epilepsy is an abnormal neurological condition characterized by recurrent seizures due to excessive electrical activity in the brain.[1] The most common symptom of epilepsy is convulsions that involve involuntary muscle contractions. Focal epilepsy is defined as seizures that initially affect limited brain regions and, in some cases, they progress to generalized seizures by the expansion of seizure-related areas and are termed focal-to-bilateral tonic-clonic seizures (FBTCSs).[2,3] The presence of FBTCS is reportedly the most significant risk factor for sudden unexpected death in epilepsy (SUDEP).[4–6] On the other hand, 6.4%–34.5% of patients with epilepsy have generalized-onset seizures that affect the whole or a large part of the brain from disease onset.[7] Moreover, 20%–30% of patients have refractory epilepsy that is resistant to the currently available pharmacological interventions. However, the elucidation of the biological mechanisms underlying epileptogenesis in humans is still limited.

Synapses are essential microstructures for the transmission of information from one neuron to another. Synaptic malfunction is considered to underlie the pathogenesis of neuropsychiatric

Table 1. Patient characteristics

	Focal-onset seizures without generalized seizures (n = 5)	Focal-to-bilateral tonic-clonic seizure (n = 17)	Generalized-onset seizure (n = 8)	F value	p
Age, years	36.6 ± 7.2	35.71 ± 10.79	30.13 ± 8.52	0.9552	0.3974
Gender (male/female)	5/0	17/0	8/0	–	–
Age at epilepsy onset, years	20.4 ± 7.78	17.88 ± 13.39	17.25 ± 5.31	0.1245	0.8834
Duration of epilepsy, years	16.4 ± 9.79	17.41 ± 12.58	11.5 ± 10.42	0.6465	0.5318
Family history	0/3	3/16	3/8	–	–
Seizure type					
FIAS	2	0	0	–	
FIAS/FAS	3	0	0		
FIAS + FBTCS	0	12	0		
FAS + FBTCS	0	3	0		
FIAS/FAS + FBTCS	0	2	0		
FBTCS	0	0	0		
GOTC	0	0	8		

Continuous variables are presented as the mean ± standard deviation. Family history refers to whether a relative has a history of epilepsy or febrile seizures. The number on the left shows the number of people with a family history and one on the right shows the number of people whose family history could be obtained (some cases missing family history). For continuous variables, one-way ANOVAs were conducted. There is no significant difference in age, gender, age at epilepsy onset, or duration of epilepsy among the three groups. FIAS, focal impaired-awareness seizure; FAS, focal aware seizure; FBTCS, focal-to-bilateral tonic-clonic seizure; GOTC, generalized-onset tonic-clonic.

disorders.[8] Despite a large number of studies on patients with epilepsy using modalities such as magnetic resonance imaging (MRI), fluorodeoxyglucose-positron emission tomography, and electroencephalogram (EEG), the synaptic characteristics of epileptogenesis are still poorly elucidated.[9–11]

Hebbian and homeostatic synaptic plasticity are major forms of neuronal plasticity in the brain.[12,13] Hebbian forms of plasticity function in an input-specific fashion by the correlated firing of pre- and postsynaptic neurons (e.g., long-term potentiation [LTP] and spike-timing-dependent plasticity).[14] On the other hand, homeostatic synaptic plasticity counteracts the global increase or decrease in neuronal activity and restrains activity within the physiological range.[15,16] The excitatory glutamate α-amino-3-hydroxy-5-methyl-4-isoxazole propionic acid receptors (AMPARs) play a pivotal role in the synaptic plasticity of the brain.[17,18] For example, the induction of LTP, one of the most well-characterized forms of Hebbian synaptic plasticity, drives AMPARs into specific synapses activated during LTP, and the same molecular synaptic modification occurs in experience-dependent synaptic plasticity *in vivo*.[18–28] The homeostatic regulation of synaptic function and scaling is induced as a compensatory change in the synaptic content of AMPARs in response to global upregulation or downregulation of neuronal activity.[17,29] Malfunction of synaptic plasticity is considered to underlie epileptogenesis.[30] In fact, AMPARs are known to be involved in epileptogenesis. It was previously reported that epileptogenic focus tissue contains an increased amount of AMPARs.[31] Furthermore, perampanel, a selective non-competitive antagonist of AMPARs, decreased seizure frequency.[32,33] However, the dynamics of AMPARs in living patients with epilepsy have not been elucidated due to the lack of technology to visualize and quantify the density of AMPARs in the living human brain. We have recently developed a positron emission tomography (PET) tracer for AMPARs that can quantify the density of AMPARs in the living human brain ([^{11}C]K-2).[34,35] This tracer enables us to investigate the relationship between the density of AMPARs and the dynamic electrical activity in the brain as measured by EEG. The tracer has been proven to be safe for application in humans.[36] Moreover, the images of the tracer represent cell-surface AMPARs, which contribute to crucial physiological functions.[37]

Here, we investigated epileptic brain functions using cross-sectional PET imaging with [^{11}C]K-2 to assess AMPAR-mediated synaptic functions and scalp EEG under resting closed-eye conditions, which reflects the ongoing dynamism of neuronal activity. We imaged 30 patients with epilepsy and 31 healthy controls using [^{11}C]K-2, which represented the density of cell-surface AMPARs (Table 1). In patients with focal-onset seizures, pathologically increased trafficking of cell-surface AMPARs enhances the amplitude of gamma activity detected by scalp EEG in the resting state, which is assumed to be pathophysiological brain activity related to epileptic seizures.[38–42] This pathological increase in the trafficking of AMPARs could result from Hebbian-type plasticity due to the potential simultaneous activation of multiple neurons. On the other hand, there was a decrease in AMPARs on the cell surface coupled with increased amplitude of gamma activity in patients with generalized-onset seizures, which could be due to compensational synaptic scaling to downregulate the neuronal overactivation. Interestingly, brain areas with AMPAR-coupled changes in the amplitude of theta activity, which is also assumed to be another brain activity associated with pathophysiological neural conditions at rest (i.e., at eyes closed condition), were apparently larger in patients with FBTCSs than in those with focal-onset seizures without generalized seizures. Compared with healthy controls, cell-surface AMPARs were decreased in larger areas of the cortex in patients with generalized seizures than in those with focal-onset seizures,

CellPress
OPEN ACCESS

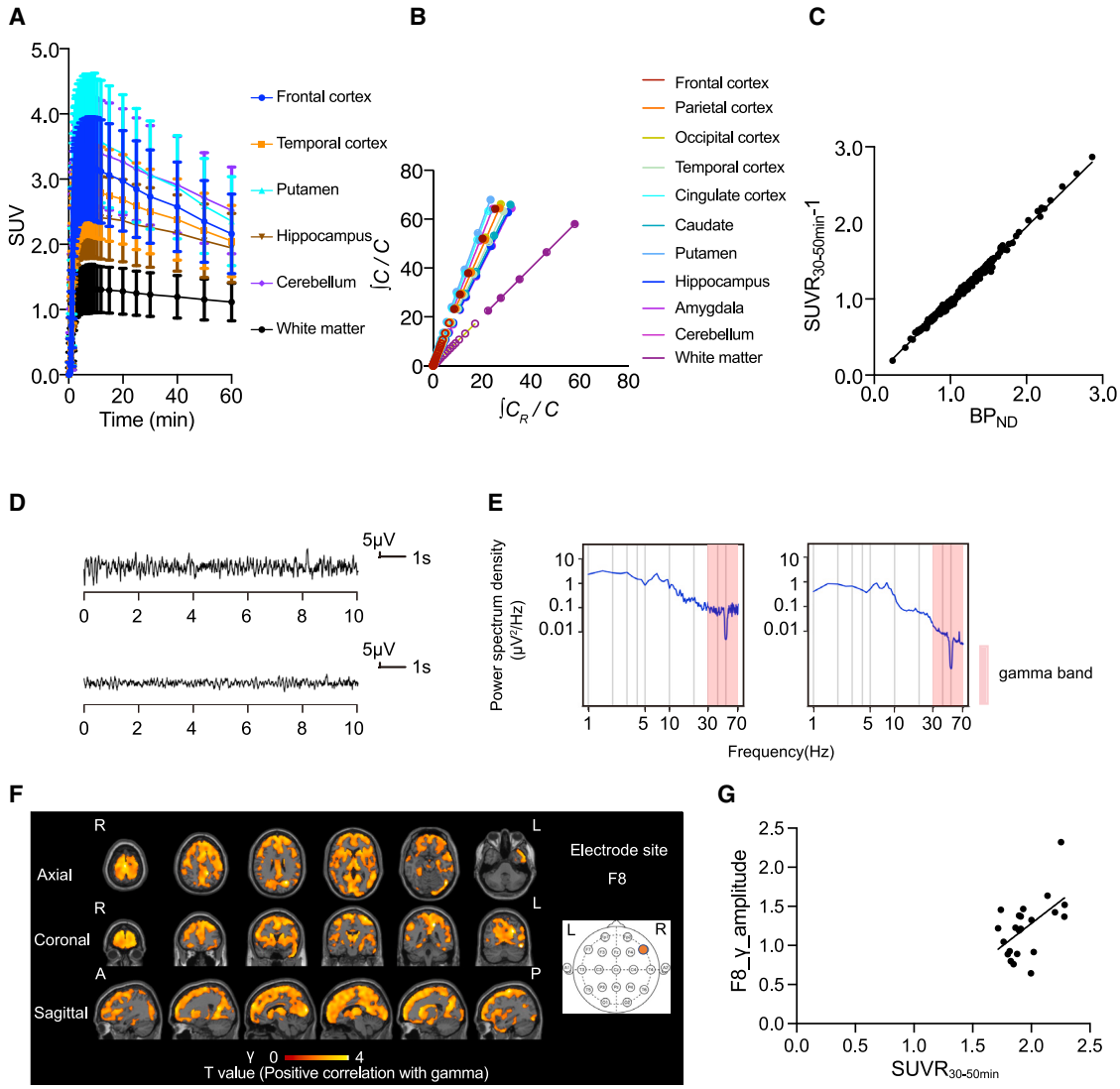

Figure 1. PET imaging characteristics of [^{11}C]K-2 and positive correlation between the amount of cell-surface AMPARs and the amplitude of gamma activity in patients with the focal-onset seizures

(A) Averaged TACs in the brains of patients with the focal-onset seizures (n = 22). The analysis was performed on 10 brain regions from a whole brain region, of which 6 representative regions are shown. Data are shown as the mean ± SD.

(B) Logan graphical analysis (LGA) plot showing the ratio between an integrated tissue TAC in the reference region (white matter; C_R) and a tissue TAC (C) (x axis) plotted against the ratio of integrated C with C itself (y axis).

(C) Correlation between $SUVR_{30–50\ min} - 1$ and BP_{ND} obtained from LGA in 10 brain regions with focal-onset seizures (n = 22; two-tailed Spearman correlation analysis: correlation coefficient = 0.996, $p < 0.0001$, $y = 0.9866x - 0.02555$). Each spot represents BP_{ND} (x axis) and the $SUVR_{30–50\ min} - 1$ (y axis), which was obtained from 10 brain regions of each patient.

(D) The EEG law data in the patients with the focal-onset seizures with the highest (top) and lowest (bottom) gamma power at the F8 electrode that correlated with $SUVR_{30–50\ min}$.

(E) The power spectrum density in the patients with the focal-onset seizures with the highest (left) and lowest (right) gamma power at the F8 electrode that correlated with $SUVR_{30–50\ min}$. The power spectral density of the EEG was calculated by averaging short-time Fourier transforms of 2-s moving windows.

(F) SPM analysis of [^{11}C]K-2 in patients with the focal-onset seizures identifies the brain regions showing a significant positive correlation between $SUVR_{30–50\ min}$ with white matter as a reference and the amplitude of gamma activity in the F8 electrode site ($p < 0.05$, $T > 1.72$, one-tailed, FDRc [false discovery rate correction]). Color scale bar indicates T value of this correlation. R, right side; L, left side; A, anterior side; P, posterior side.

(G) Scatterplot analysis of [^{11}C]K-2 in patients with focal-onset seizures shows strong positive correlation between [^{11}C]K-2 $SUVR_{30–50\ min}$ of colored region in (F) and the amplitude of gamma activity in the F8 electrode site (n = 22, Spearman correlation analysis; correlation coefficient = 0.4828, p = 0.0229). Each spot corresponds to $SUVR_{30–50\ min}$ (x axis) and the amplitude of the gamma activity at F8 (y axis) of a single patient, and 22 spots obtained from 22 patients are displayed.

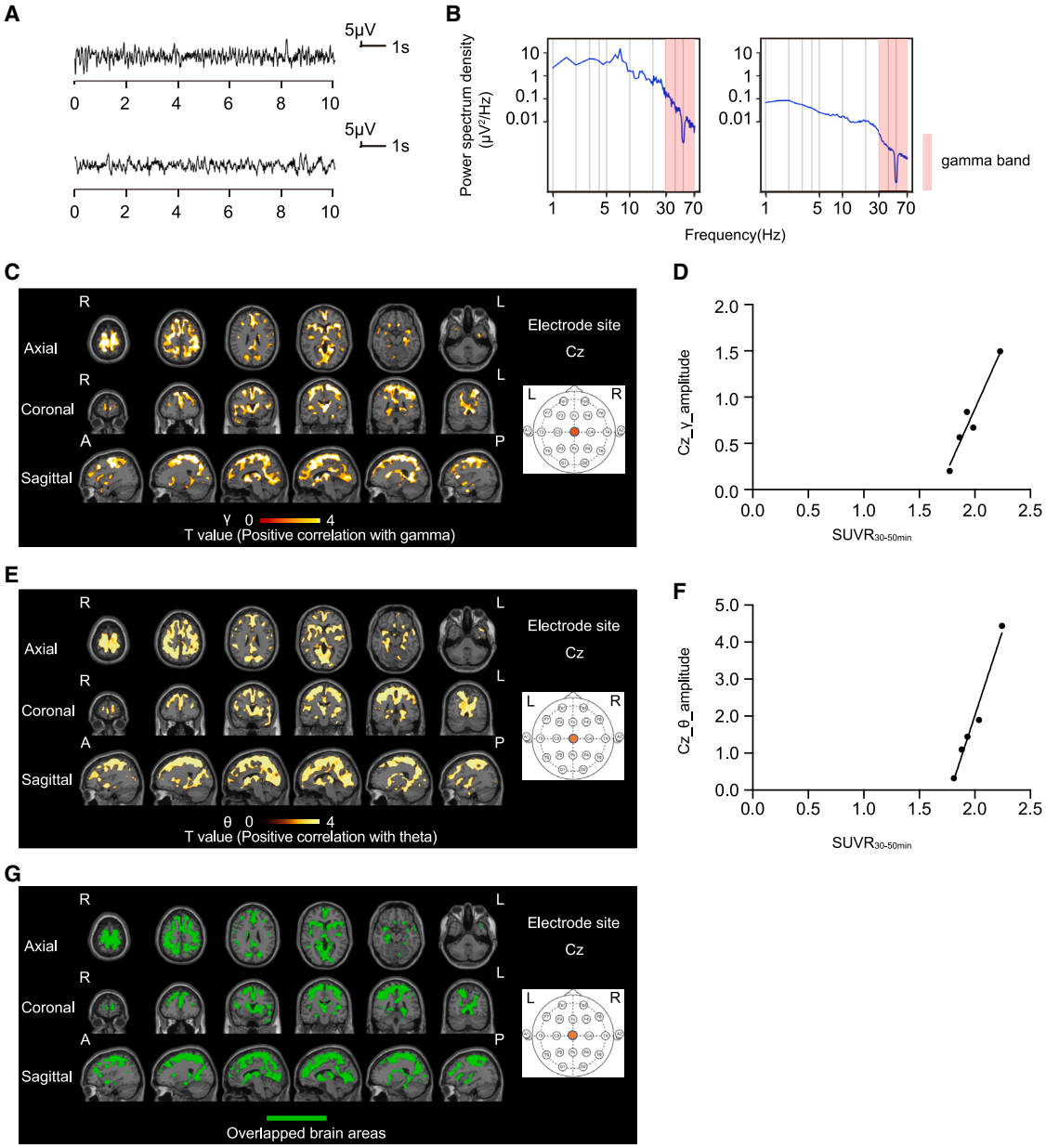

Figure 2. Positive AMPAR-gamma and theta activity couplings are observed in patients with focal-onset seizures without generalized seizure

(A) The EEG law data in the patients with the focal-onset seizures without generalized seizure with the highest (top) and lowest (bottom) gamma power at the Cz electrode that correlated with $SUVR_{30–50\ min}$.

(B) The power spectrum density in the patients with the focal-onset seizures without generalized seizure with the highest (left) and lowest (right) gamma power at the Cz electrode that correlated with $SUVR_{30–50\ min}$. The power spectral density of the EEG was calculated by averaging short-time Fourier transforms of 2-s moving windows.

(C) SPM analysis of [^{11}C]K-2 in patients with the focal-onset seizures without generalized seizure identifies the brain regions showing a significant positive correlation between $SUVR_{30–50\ min}$ with white matter as a reference and the amplitude of gamma activity in the Cz electrode site ($p < 0.05$, $T > 2.35$, one-tailed, FDRc). Color scale bar indicates T value of this correlation. R, right side; L, left side; A, anterior side; P, posterior side.

(D) Scatterplot analysis of [^{11}C]K-2 in patients with focal-onset seizures without generalized seizure shows strong positive correlation between [^{11}C]K-2 $SUVR_{30–50\ min}$ of the colored region in (C) and the amplitude of gamma activity in the Cz electrode site ($n = 5$, Pearson correlation analysis; correlation coefficient = 0.9668, $p = 0.0072$). Each spot corresponds to $SUVR_{30–50\ min}$ (x axis) and the amplitude of the gamma activity at Cz (y axis) of single patient, and five spots obtained from five patients are displayed.

(E) SPM analysis of [^{11}C]K-2 in patients with focal-onset seizures without generalized seizure identifies brain regions showing a significant positive correlation between $SUVR_{30–50\ min}$ with white matter as a reference and the amplitude of theta activity in the Cz electrode site ($p < 0.05$, $T > 2.35$, one-tailed, FDRc). Color scale bar indicates T value of this correlation. R, right side; L, left side; A, anterior side; P, posterior side.

(legend continued on next page)

which can also be due to the homeostatic synaptic scaling induced by neuronal overactivation. Therefore, Hebbian plasticity to increase trafficking of AMPARs and homeostatic scaling for the compensatory downregulation of synaptic function in seizures could regulate epileptic brain function.

RESULTS

Positive correlation between cell-surface AMPAR density and the amplitude of gamma activity in focal epilepsy

To investigate the synaptic basis of epilepsy, we first performed PET scan for 22 patients with focal-onset seizures using [^{11}C]K-2, in combination with scalp EEG using 19 electrodes in the resting state (eyes closed). As previously observed for healthy controls,[34] time-activity curves (TACs) from multiple brain regions of [^{11}C]K-2-injected patients with focal-onset seizures showed rapid radiotracer uptake in the brain and regional heterogeneity. The lowest radioactivity was observed in the white matter (WM), where no AMPARs were detected (Figure 1A).[34] Logan graphical analysis (LGA) using WM as a reference showed linearity, indicating the reversible binding kinetics of [^{11}C]K-2 in patients with focal-onset seizures, as observed in healthy controls in our previous study[34] (Figure 1B). Based on LGA, we calculated the non-displaceable binding potential (BP_{ND}), which is a quantitative index of receptor density utilized in PET receptor imaging.[43] To investigate the regional uptake of [^{11}C]K-2 in patients with focal-onset seizures, we utilized the standardized uptake value ratio $(SUVR)_{30–50\ min}$ with WM as a reference. There was a good linear relationship between BP_{ND} and $SUVR_{30\text{-}50\ min} - 1$ (Figure 1C). Thus, we utilized $SUVR_{30\text{-}50\ min}$ for further analysis. Voxel-wise analysis was performed using Statistical Parametric Mapping (SPM) 12. In patients with focal-onset seizures, we found a significant positive correlation between $SUVR_{30\text{-}50\ min}$ and the amplitude of gamma activity (positive AMPAR-gamma activity coupling) in a large part of cortical areas such as the precentral gyrus, supplementary motor area, superior parietal lobule, precuneus, thalamus, and cingulum (Figures 1D–1G and S1).

Spread of AMPAR-coupled theta activity changes underlies progression to FBTCS

Next, we investigated the mechanisms underlying progression to FBTCSs from focal-onset seizures without generalized seizures. In 22 patients with focal-onset seizures, we compared PET images with [^{11}C]K-2 of 5 patients without generalized seizures and 17 patients with FBTCSs in relation to the electrical activity obtained from scalp EEG (Tables S1 and S2). In 5 patients with focal-onset seizures without generalized seizures, we detected brain areas with positive AMPAR-gamma activity coupling similar to those observed in the 22 patients with focal-onset seizures (Figures 2A–2D and S2). In these patients, we observed a significant positive correlation between $SUVR_{30–50\ min}$ and the amplitude of the theta activity (positive AMPAR-theta activity coupling) in almost overlapping brain areas with positive AMPAR-gamma activity coupling (at multiple electrodes such as Cz and T5) (Figures 2C–2G, S2, and S3). By scanning 17 patients with FBTCSs, we detected positive AMPAR-gamma activity coupling at the F8 electrode site in brain areas similar to those observed in the analysis of 5 patients with focal-onset seizures without generalization (Figures 2A–2D and 3A–3D). Interestingly, we found a significant negative correlation between $SUVR_{30–50\ min}$ and the amplitude of theta activity (negative AMPAR-theta activity coupling) in the brain areas at the T5 electrode site, complementary to the above-mentioned brain areas that exhibited positive AMPAR-gamma activity coupling at the F8 electrode site (these two regions were minimally overlapped; Figure 3G), while no brain areas with positive AMPAR-theta activity coupling were detected in patients with FBTCSs. Further, abnormal gamma and theta activities were detected in different electrode sites in accordance with the spread of epileptic electrical activity in the FBTCS (Figures 3A–3G). These results suggest that the disappearance of positive AMPAR-theta activity coupling and the spread of negative AMPAR-theta activity coupling underlie the transition from focal to generalized seizures.

Generalized-onset seizure downregulates AMPAR levels

A total of eight patients with generalized-onset seizures were PET scanned using [^{11}C]K-2 (Table S3). TACs from multiple brain regions of [^{11}C]K-2-injected patients with generalized-onset seizures showed rapid radiotracer uptake in the brain and regional heterogeneity, with the lowest radioactivity observed in the WM (Figure 4A). LGA using WM as a reference showed linearity, indicating the reversible binding kinetics of [^{11}C]K-2 in patients with generalized-onset seizures (Figure 4B). Based on LGA, we calculated the BP_{ND}. Furthermore, patients with generalized-onset seizures showed a good linear relationship between BP_{ND} and $SUVR_{30–50\ min}$ (Figure 4C). We found a significant negative correlation between $SUVR_{30–50\ min}$ and the amplitude of gamma activity (negative AMPAR-gamma activity coupling) in a large part of cortical areas, such as superior frontal gyrus, angular gyrus, precuneus, superior parietal lobule, middle frontal gyrus, postcentral gyrus, and inferior parietal lobule occipital, with multiple electrode sites (Figures 4D–4G and S4). Multiple electrodes detected negative AMPAR-gamma activity coupling in almost identical areas. We did not observe any brain areas with a correlation between $SUVR_{30–50\ min}$ and the amplitude of theta activity.

Regional decrease in AMPARs in patients with epilepsy compared with healthy controls

To compare AMPAR distributions in patients with epilepsy with those in healthy controls, we used voxel-wise analysis using SPM to compare the $SUVR_{30–50\ min}$ of [^{11}C]K-2 using WM as a

(F) Scatterplot analysis of [^{11}C]K-2 in patients with focal-onset seizures without generalized seizure shows strong positive correlation between [^{11}C]K-2 $SUVR_{30–50\ min}$ of colored region in (E) and the amplitude of theta activity in the Cz electrode site (n = 5, Pearson correlation analysis; correlation coefficient = 0.9862, p = 0.002). Each spot corresponds to $SUVR_{30–50\ min}$ (x axis) and the amplitude of the theta activity at Cz (y axis) of single patient, and five spots obtained from five patients are displayed.

(G) The brain regions of positive AMPAR-gamma activity coupling shown in (C) and positive AMPAR-theta activity coupling shown in (E) are mostly overlapped (highlighted by green color without scale) in patients with focal seizures without generalized seizure. R, right side; L, left side; A, anterior side; P, posterior side.

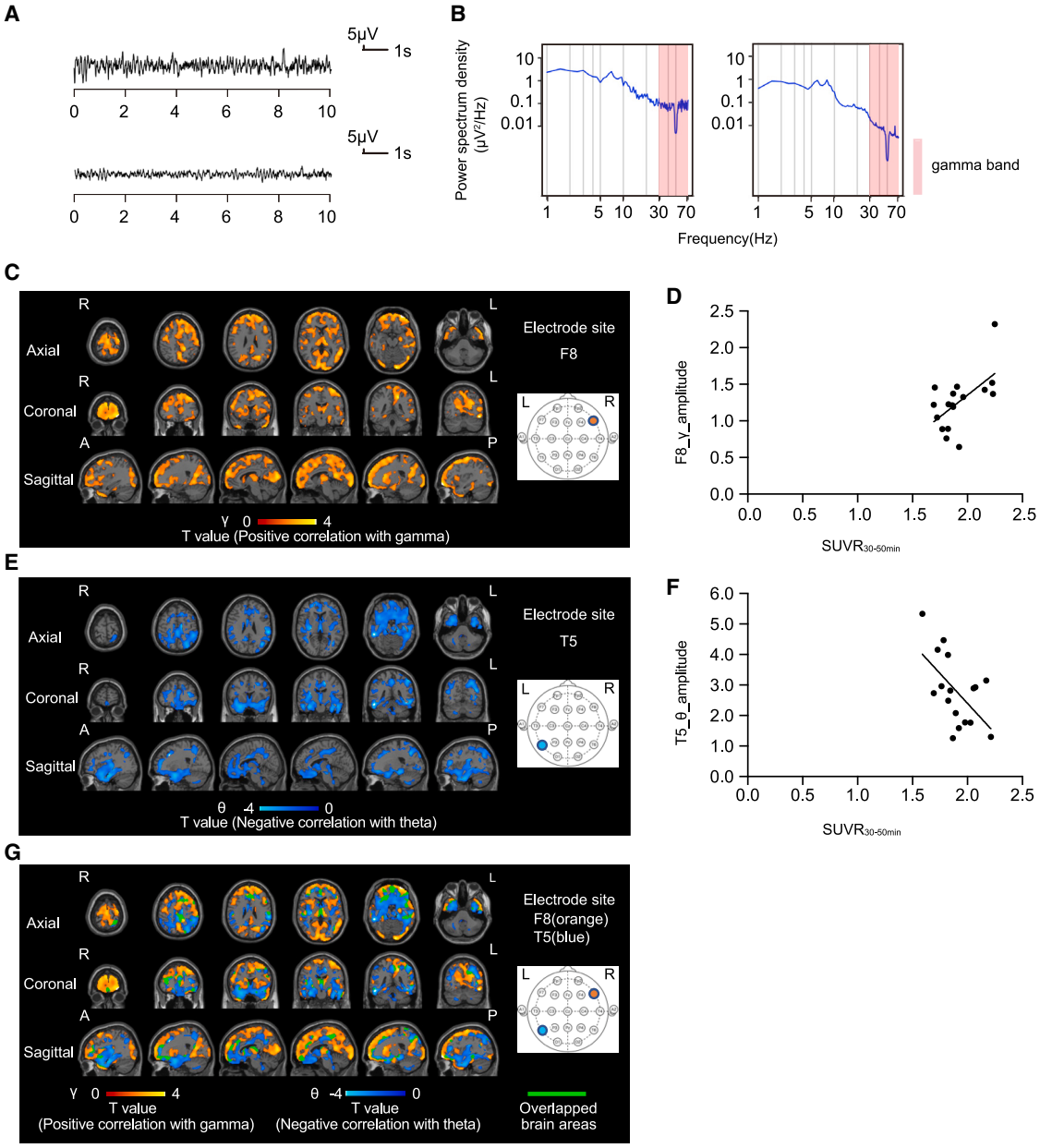

Figure 3. Spread of AMPAR-coupled theta activity changes underlies the progression to FBTCS

(A) The EEG law data in the patient with FBTCs with the highest (top) and lowest (bottom) gamma power at the F8 electrode that correlated with $SUVR_{30–50\ min}$.

(B) The power spectrum density in the patient with FBTCSs with the highest (left) and lowest (right) gamma power at the F8 electrode that correlated with $SUVR_{30–50\ min}$. The power spectral density of the EEG was calculated by averaging short-time Fourier transforms of 2-s moving windows.

(C) SPM analysis of [^{11}C]K-2 in patients with FBTCSs identifies the brain regions showing a significant positive correlation between $SUVR_{30–50\ min}$ with white matter as a reference and the amplitude of gamma activity in the F8 electrode site ($p < 0.05$, $T > 1.49$, one-tailed, FDRc). Color scale bar indicates T value of this correlation. R, right side; L, left side; A, anterior side; P, posterior side.

(D) Scatterplot analysis of [^{11}C]K-2 in patients with the FBTCSs shows strong positive correlation between [^{11}C]K-2 $SUVR_{30–50\ min}$ of colored region in (C) and the amplitude of gamma activity in the F8 electrode site ($n = 17$, Spearman correlation analysis; correlation coefficient = 0.5074, $p = 0.0397$). Each spot corresponds to $SUVR_{30–50\ min}$ (x axis) and the amplitude of the gamma activity at F8 (y axis) of a single patient, and 17 spots obtained from 17 patients are displayed.

(E) SPM analysis of [^{11}C]K-2 in patients with FBTCSs identifies the brain regions showing a significant negative correlation between $SUVR_{30–50\ min}$ with white matter as a reference and the amplitude of theta activity in the T5 electrode site ($p < 0.05$, $T > 1.49$, one-tailed, FDRc). Color scale bar indicates T value of this correlation. R, right side; L, left side; A, anterior side; P, posterior side.

(F) Scatterplot analysis of [^{11}C]K-2 in patients with FBTCSs shows strong negative correlation between [^{11}C]K-2 $SUVR_{30–50\ min}$ of colored region in (E) and the amplitude of theta activity in the T5 electrode site ($n = 17$, Pearson correlation analysis; correlation coefficient = −0.5764, $p = 0.0154$). Each spot corresponds to $SUVR_{30–50\ min}$ (x axis) and the amplitude of the theta activity at T5 (y axis) of single patient, and 17 spots obtained from 17 patients are displayed.

(legend continued on next page)

reference. We scanned 31 healthy controls and constructed the $SUVR_{30–50\ min}$ using WM as a reference. In patients with focal-onset seizures, we detected a decrease in cell-surface AMPARs in large cortical areas compared with those in healthy controls (Figures 5A–5D). Only limited areas with decreased cell-surface AMPARs overlapped with those exhibiting positive AMPAR-gamma activity coupling or positive AMPAR-theta activity coupling in patients with focal-onset seizures without generalized seizure (Figure 5E). Similarly, in patients with FBTCSs, brain areas with decreased cell-surface AMPARs were minimally overlapped with those with positive AMPAR-gamma activity coupling or negative AMPAR-theta activity coupling (Figure 5F). Thus, cell-surface AMPARs were reduced compared with healthy subjects in brain areas that did not produce AMPAR-mediated epileptic activity. In patients with focal-onset seizures, we observed larger brain areas with decreased cell-surface AMPARs in patients with FBTCSs than in those without progression to generalized seizures (Figures 5A and 5C). In patients with generalized-onset seizures, we observed decreased cell-surface AMPARs in large cortical areas compared with healthy controls, and these areas overlapped well with the negative AMPAR-gamma activity coupling regions (Figures 5G–5I). The areas of reduced cell-surface AMPARs in patients with generalized-onset seizures were larger than those in patients with focal-onset seizures (Figures 5A, 5C, and 5G). We did not detect any brain regions with higher AMPAR levels in patients with epilepsy compared with healthy controls, which also indicates that the physiological fraction of AMPARs can be widely decreased in the epileptic brain. Based on these results, we hypothesized that, in patients with focal-onset seizures, functional (physiological) AMPARs (which can control normal brain functions such as learning, behavior, and information processing) can be downregulated for compensation potentially via homeostatic scaling without coupling with epileptic activity, while compensational decrease in cell-surface AMPARs can couple with abnormal electrical activity in patients with generalized-onset seizures for whom epileptic discharge can be induced by other causes, such as abnormal sodium, potassium, or calcium channel functions, rather than the abnormality in AMPAR-mediated excitatory synapses.[44,45] In line with our hypothesis, we wondered if homeostatic scaling-induced downregulation of cell-surface AMPARs also occurs in brain areas with positive AMPAR-gamma activity coupling in patients with focal-onset seizures. We estimated the physiological fraction of cell-surface AMPARs in brain areas with positive AMPAR-gamma activity coupling. We compared $SUVR_{30–50\ min}$ values between patients with focal epilepsy and healthy controls after adjusting for the gamma activity amplitude. Using data from 31 healthy controls and 22 patients with focal epilepsy, we performed multivariate regression analysis with $SUVR_{30–50\ min}$ as the objective variable and disease status (healthy or epileptic) and gamma activity amplitude as explanatory variables. In this regression analysis, the gamma activity amplitudes for all healthy controls were considered to be zero.[46,47] Thus, the $SUVR_{30–50\ min}$ of patients with focal epilepsy when the gamma activity amplitudes were adjusted to zero could be interpreted as the fraction of cell-surface AMPARs that contributed to physiological function in these regions of the patients (Figure 5J). We found that the estimated physiological fraction of cell-surface AMPARs in the brain regions generating gamma activity was significantly lower than that of healthy controls in the same brain regions.

DISCUSSION

Here, we revealed the biological basis of epilepsy by combining PET imaging for AMPARs and EEG in 30 patients with epilepsy. In patients with focal-onset seizures, a pathological increase in cell-surface AMPARs in large parts of cortical areas enhanced excitatory epileptic activity. Hebbian plasticity to induce trafficking of AMPARs caused by potential simultaneous firing of multiple neurons could underlie the accumulation of pathological cell-surface AMPARs, resulting in the increase in the amplitude of gamma activity, which reflects augmentation of excitability in patients with focal-onset seizures. In contrast, patients with generalized-onset seizures had negative AMPAR-gamma activity coupling in the cortex, which could result from compensatory downregulation of AMPAR via internalization (potential homeostatic scaling) due to epileptic long-term global neuronal firing.

We detected a reduction in cell surface AMPARs in various brain regions in patients with focal- and generalized-onset seizures compared with healthy controls. Reduced AMPARs in epileptic brains could be compensational synaptic changes to downregulate global neuronal activity in the epileptic brain. The areas of decreased cell-surface AMPARs in patients with generalized-onset seizures compared with healthy controls were larger than those in patients with focal-onset seizures. This indicates that increased compensation in generalized-onset seizures compared with focal-onset seizures could induce widespread reduction in AMPARs in the generalized-onset seizures. Furthermore, while the reduction in cell-surface AMPARs was not coupled with the amplitude of gamma activity in patients with focal-onset seizures, we detected negative AMPAR-gamma activity coupling in brain areas of patients with generalized-onset seizures and observed a reduction in cell-surface AMPARs compared with those in healthy controls. Thus, in generalized-onset seizure, global elevation of activity presumably due to causes other than post-synaptic increase in AMPARs, such as malfunction of sodium channels,[48,49] can lead to an enhancement in the amplitude of gamma activity by the augmented presynaptic inputs. This may induce compensative reduction of post-synaptic AMPARs, resulting in a negative AMPAR gamma activity coupling. The involvement of interneuron activity could contribute to this correlation in the generalized-onset seizure. For example, if excitatory inputs onto interneurons are reduced, the activity of the interneurons is decreased and could result in an increase in the amplitude of gamma waves. Considering the

(G) The brain regions of positive AMPAR-gamma activity coupling shown in (C) and negative AMPAR-theta activity coupling shown in (E) are complementary (note that overlapped regions highlighted by green color are limited) in patients with FBTCSs. Orange scale bar indicates T value of positive AMPAR-gamma activity coupling and blue scale bar indicates T value of negative AMPAR-theta activity coupling. R, right side; L, left side; A, anterior side; P, posterior side.

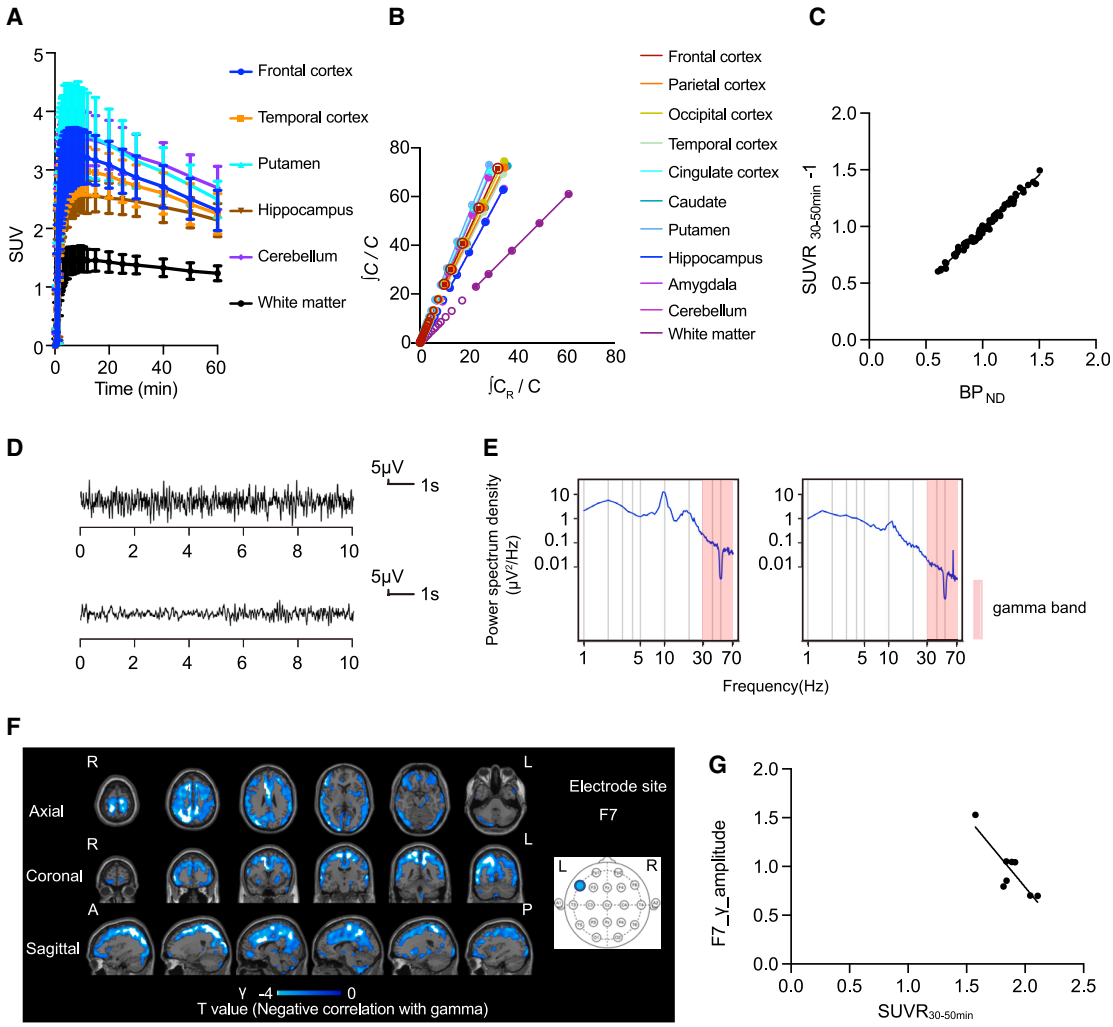

Figure 4. Generalized-onset seizure downregulates AMPAR levels

(A) Averaged TACs in the brains of patients with the generalized-onset seizures (n = 7). The analysis was performed on 10 brain regions in the whole brain, of which 6 representative regions are shown. Data are shown as the mean ± SD.

(B) Logan graphical analysis (LGA) plot showing the ratio between an integrated tissue TAC in the reference region (white matter; C_R) and a tissue TAC (C) (x axis) plotted against the ratio of integrated C with C itself (y axis).

(C) Correlation between $SUVR_{30–50\ min} - 1$ and BP_{ND} obtained from LGA in 10 brain regions with generalized-onset seizures (n = 7; two-tailed Pearson correlation analysis: correlation coefficient = 0.9932, $p < 0.0001$, $y = 0.955x + 0.02278$). Each spot represents BP_{ND} (x axis) and the $SUVR_{30–50\ min} - 1$ (y axis) that was obtained from 10 brain regions of each patient.

(D) The EEG law data in the patients with the generalized-onset seizures with the highest (top) and lowest (bottom) gamma power at the F7 electrode that correlated with $SUVR_{30–50\ min}$.

(E) The power spectrum density in the patients with the generalized-onset seizures with the highest (left) and lowest (right) gamma power at the F7 electrode that correlated with $SUVR_{30–50\ min}$. The power spectral density of the EEG was calculated by averaging short-time Fourier transforms of 2-s moving windows.

(F) SPM analysis of [^{11}C]K-2 in patients with the generalized-onset seizures identifies the brain regions showing a significant negative correlation between $SUVR_{30–50\ min}$ with white matter as a reference and the amplitude of gamma activity in the F7 electrode site ($p < 0.05$, $T > 1.94$, one-tailed, FDRc). Color scale bar indicates T value of this correlation. R, right side; L, left side; A, anterior side; P, posterior side.

(G) Scatterplot analysis of [^{11}C]K-2 in patients with generalized-onset seizures shows strong negative correlation between [^{11}C]K-2 $SUVR_{30–50\ min}$ of the colored region in (F) and the amplitude of gamma activity in the F7 electrode site (n = 8, Pearson correlation analysis; correlation coefficient = −0.851, p = 0.0074). Each spot corresponds to $SUVR_{30–50\ min}$ (x axis) and the amplitude of the gamma activity at F7 (y axis) of a single patient, and eight spots obtained from eight patients are displayed.

small fraction of AMPARs in interneurons (approximately >80% of excitatory inputs are onto pyramidal neurons in humans[50]), these two events could contribute to the negative correlation between the amplitude of the gamma wave and the density of AMPARs in the generalized-onset seizure.

Physiological and pathological fractions of AMPARs can be found in patients with epilepsy. In epilepsy, we only detected brain areas with reduced cell-surface AMPARs compared with those in healthy controls. Thus, compensational downregulation of AMPARs in epilepsy might occur in the physiological fraction of

CellPress
OPEN ACCESS

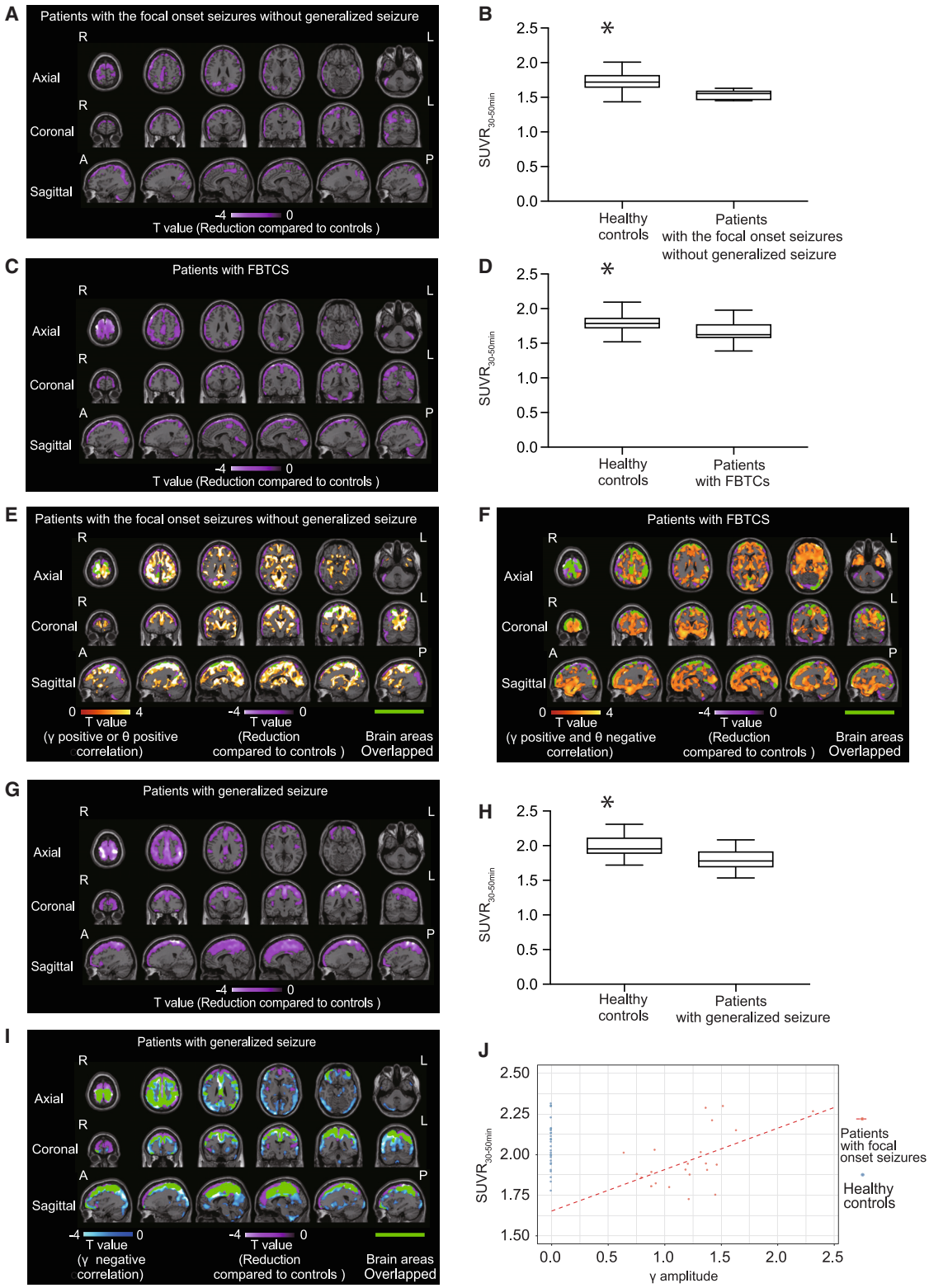

Figure 5. Regional decrease in AMPARs in patients with epilepsy compared with healthy controls

(A) SPM analysis of [^{11}C]K-2 in patients with focal-onset seizures without generalized seizure identifies the brain regions showing a significant reduction in $SUVR_{30–50\ min}$ with white matter as a reference compared with those of healthy controls (highlighted by purple color; $p < 0.05$, $T > 1.69$, one-tailed, FDRc). Color scale bar indicates T value of the difference between two groups. R, right side; L, left side; A, anterior side; P, posterior side.

(legend continued on next page)

AMPARs, which could lead to disturbance in normal brain functions and result in intellectual disability of some patients with epilepsy.[51,52] Using [^{11}C]K-2-PET imaging, we recently reported that electric current dipoles (ECDs), identified by magnetoencephalography in surgical cases with mesial temporal lobe epilepsy, were colocalized with a high accumulation of AMPARs in brain regions showing epileptic discharges in comparison with the non-epileptic hemisphere.[35] Although we did not analyze these surgical cases in this study, asymmetrical upregulation of AMPARs colocalized with ECDs might be within the normal range due to the compensatory reduction of the physiological fraction of AMPARs in these brain regions. In patients with focal-onset seizures, we estimated the physiological fraction of cell-surface AMPARs using the plot of the correlation between $SUVR_{30–50\ min}$ and the amplitude of gamma activity. The estimated physiological fraction of AMPARs in brain regions generating gamma activity was significantly decreased in patients with focal-onset seizures compared with healthy controls. These could be due to homeostatic synaptic scaling in the physiological fraction of AMPARs in response to the epileptic excitation of the pathological fraction of AMPARs that could result from Hebbian plasticity-induced trafficking of AMPARs by the increased simultaneous neuronal firing. This suggests that two major synaptic plasticities, Hebbian plasticity and homeostatic synaptic scaling, occur in the same brain regions. This synaptic event could result in a normal range of the amount of total cell-surface AMPARs in the majority of the brain regions generating gamma activity in patients with focal-onset seizures. Decreased physiological fractions of AMPARs can lead to various neuronal dysfunctions in patients with epilepsy.[53,54] Despite potential reduction in the physiological fraction of AMPARs, downregulation of pathological AMPARs can reduce epileptic discharges and can be a potential therapeutic strategy for epilepsy.

While patients with focal-onset seizures without generalized seizure exhibited positive AMPAR-gamma and -theta activity coupling in almost overlapped brain regions, in patients with FBTCSs, we observed negative AMPAR-theta activity coupling in the brain areas complementary to regions that exhibited positive AMPAR-gamma activity coupling. The biological basis for the generation of theta activity has not been well characterized. A previous study has suggested that theta activity reflects inhibitory function on the neuron.[55–58] Based on this hypothesis, we considered the following mechanism of progression to FBTCS: in patients with focal-onset seizures without generalized seizure, pathological increase in AMPARs enhanced both excitatory and inhibitory neuronal activity in the cortical area, which could prevent progression to generalized seizures. This excitatory and inhibitory balance is disrupted in patients with FBTCSs. Brain areas with AMPAR-coupled enhancement of excitatory neuronal activity did not exhibit augmentation of inhibitory neuronal activity in accordance with the elevation of AMPARs. Furthermore, in patients with FBTCSs, large brain regions other than the areas with positive AMPAR-gamma activity coupling exhibited negative AMPAR-theta activity coupling, indicating that the spread of disinhibition was the underlying mechanism for generalized seizures that developed from focal-onset seizures (Figure 6).

Taken together, Hebbian plasticity and homeostatic synaptic scaling may differentially regulate the functions of an epileptic brain and provide a cohesive biological mechanism of epileptogenesis.

Limitations of the study

In this study, we characterized only male patients. It will be crucial to perform a similar clinical study with female patients, which can be an important addition to the current study.

(B) $SUVR_{30–50\ min}$ in reduced regions of patients with focal-onset seizures without generalized seizure compared with healthy controls (mapped in A). Data are shown as $SUVR_{30–50\ min}$ with patients with focal-onset seizures without generalized seizure and $SUVR_{30–50\ min}$ with healthy controls. *p = 0.0041 (two-tailed Mann-Whitney U test). Data are shown as the mean ± SEM.

(C) SPM analysis of [^{11}C]K-2 in patients with FBTCSs identifies the brain regions showing a significant reduction in $SUVR_{30–50\ min}$ with white matter as a reference compared with those of healthy controls (highlighted by purple color; $p < 0.05$, $T > 1.68$, one-tailed, FDRc). Color scale bar indicates T value of the difference between two groups. R, right side; L, left side; A, anterior side; P, posterior side.

(D) $SUVR_{30–50\ min}$ in reduced regions of patients with FBTCSs compared with healthy controls (mapped in C). Data are shown as $SUVR_{30–50\ min}$ with patients with FBTCSs and $SUVR_{30–50\ min}$ with healthy controls. *p = 0.0039 (two-tailed Mann-Whitney U test). Data are shown as the mean ± SEM.

(E) In patients with the focal-onset seizures without generalized seizures, the brain regions of positive AMPAR-gamma/theta activity coupling shown in Figures 2C and 2E (highlighted by orange color) and reduced AMPARs compared with healthy controls shown in (A) (highlighted by purple color) are minimally overlapped (highlighted by green color without scale). Orange scale bar indicates T value of positive AMPAR-gamma/theta activity coupling and blue scale bar indicates T value of the difference between patients and healthy controls. R, right side; L, left side; A, anterior side; P, posterior side.

(F) In patients with FBTCSs, the brain regions of positive AMPAR-gamma or negative AMPAR-theta activity coupling shown in Figures 3C and 3E (highlighted by orange color) and reduced AMPARs compared with healthy controls shown in (C) (highlighted by purple color) are moderately overlapped (highlighted by green color without scale). Orange scale bar indicates T value of positive AMPAR-gamma/negative AMPAR-theta activity coupling and purple scale bar indicates T value of the difference between patients and healthy controls. R, right side; L, left side; A, anterior side; P, posterior side.

(G) SPM analysis of [^{11}C]K-2 in patients with the generalized-onset seizures identifies the brain regions showing a significant reduction in $SUVR_{30–50\ min}$ with white matter as a reference compared with those of healthy controls (highlighted by purple color; $p < 0.05$, $T > 1.69$, one-tailed, FDRc). Color scale bar indicates T value of the difference between two groups. R, right side; L, left side; A, anterior side; P, posterior side.

(H) $SUVR_{30–50\ min}$ in reduced regions of patients with the generalized-onset seizures compared with healthy controls (mapped in G). Data are shown as $SUVR_{30–50\ min}$ patients with the generalized-onset seizures and $SUVR_{30–50\ min}$ with healthy controls. *p = 0.0053 (two-tailed Mann-Whitney U test). Data are shown as the mean ± SEM.

(I) In patients with the generalized-onset seizures, the brain regions of negative AMPAR-gamma activity coupling shown in Figure 4F (highlighted by blue color) and reduced AMPARs compared with healthy controls shown in (G) (highlighted by purple color) are broadly overlapped (highlighted by green color without scale). Blue scale bar indicates T value of negative AMPAR-gamma activity coupling and purple scale bar indicates T value of the difference between patients and healthy subjects. R, right side; L, left side; A, anterior side; P, posterior side.

(J) Scatterplot showing gamma activity amplitude and [^{11}C]K-2 $SUVR_{30–50\ min}$ in patients with focal-onset seizures and healthy controls. Red dots represent data from patients with focal-onset seizures, and blue dots represent imputed data from healthy controls whose gamma activity amplitudes are assumed to be zero (mean difference 0.388; 95% CI 0.16–0.61; p = 0.00136).

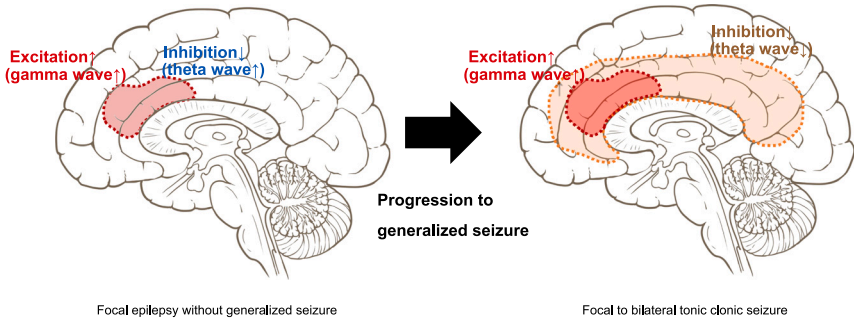

Figure 6. A potential mechanism for the progression to FBTCS: Spread of disinhibition can underlie the generalized seizure developed from focal-onset seizure

(Left) In patients with focal-onset seizures without generalized seizure, excitation is under control to some degree by the inhibition augmented by increased AMPARs in the same region where AMPAR-coupled pathological upregulation of excitation is observed. (Right) In patients with FBTCSs, AMPAR-coupled disinhibition is considered to spread in the brain, which can shift from focal to generalized seizures.

STAR★METHODS

Detailed methods are provided in the online version of this paper and include the following:

- KEY RESOURCES TABLE
- RESOURCE AVAILABILITY
  - Lead contact
  - Materials availability
  - Data and code availability
- EXPERIMENTAL MODEL AND SUBJECT DETAILS
  - Ethics statement
  - Human participants
  - Scalp-electroencephalogram
  - *In vivo* PET and MRI imaging
- METHOD DETAILS
  - Acquisition of tissue time activity curve
  - Logan graphical analysis
  - PET and MRI imaging procedure
  - Imaging data analysis
- QUANTIFICATION AND STATICAL ANALYSIS
  - Correlation between $SUVR_{30\text{-}50}$ min and EEG amplitude
  - Comparison of $SUVR_{30\text{-}50}$ min values between healthy controls and patients with epilepsy
- ADDITIONAL RESOURCES

SUPPLEMENTAL INFORMATION

Supplemental information can be found online at https://doi.org/10.1016/j.xcrm.2023.101020.

ACKNOWLEDGMENTS

The authors acknowledge Osato Iwata, Toshiro Miyauchi, Keiko Hara, Tomokatsu Hori, and Ichiro Takumi for recruiting patients. This project was supported by funds from Eisai (T.T.) and the Japan Agency for Medical Research and Development (AMED) under grant JP20dm0107124 (T.T.). This project was partially supported by the Japan Agency for Medical Research and Development (AMED) under grants JP18dm0207023 (T.T.), JP22dm0207072 (T.T.), and JP19lm0203007 (T.T.); the Japan Society for the Promotion of Science KAKENHI under grant 20H05922 (T.T.); and a grant from the Takeda Science Foundation (T.T.).

AUTHOR CONTRIBUTIONS

T.T. designed and organized the project and established scientific concepts based on interpretation of the data in this study. T.T. wrote the manuscript's main framework. T.T., Tomoyuki Miyazaki, E.T., and T. Mihara wrote the manuscript. Tomoyuki Miyazaki and T.E. wrote the clinical protocol based on scientific concepts, and T.T. designed the study. T.E., M.H., W.N., and Y.K. analyzed the PET imaging data. T.E., Y.N., and Takahiro Miyazaki analyzed the EEG data. Tomoyuki Miyazaki, M.I., H.U., and K. Kanai organized the recruitment of patients. Y. Takayama, N.I., A.H., A.S., K.N., H.T., N.N., T.K., S.N., M.M., N.M., and H.I. contributed to on-site patient management. T.T., Tomoyuki Miyazaki, E.T., Y.H., R.M., and A.I. interpreted the data. T.A., Y. Takada, and K. Kimura synthesized the [^{11}C]K-2. All the authors discussed the results and commented on the manuscript.

DECLARATION OF INTERESTS

T.T. and T.M. are the inventors on a patent application claiming a novel compound that specifically binds to the AMPA receptor, which includes [^{11}C]K-2. The patent used in this work is "Novel compound that specifically binds to AMPA receptor" (WO/2017/006931) and was filed with the Shobayashi International Patent and Trademark Office.

INCLUSION AND DIVERSITY

We support inclusive, diverse, and equitable conduct of research.

Received: December 7, 2022
Revised: February 8, 2023
Accepted: March 22, 2023
Published: April 19, 2023

REFERENCES

1. Chen, Z., Brodie, M.J., Liew, D., and Kwan, P. (2018). Treatment outcomes in patients with newly diagnosed epilepsy treated with established and new antiepileptic drugs: a 30-year longitudinal cohort study. JAMA Neurol. *75*, 279–286. https://doi.org/10.1001/jamaneurol.2017.3949.
2. Christie, H., D'Souza, W., Cook, M., and Seneviratne, U. (2021). Can semiology differentiate between bilateral tonic-clonic seizures of focal-onset and generalized-onset? A systematic review. Epilepsy Behav. *116*, 107769. https://doi.org/10.1016/j.yebeh.2021.107769.
3. Falco-Walter, J.J., Scheffer, I.E., and Fisher, R.S. (2018). The new definition and classification of seizures and epilepsy. Epilepsy Res. *139*, 73–79. https://doi.org/10.1016/j.eplepsyres.2017.11.015.
4. Park, K.J., Sharma, G., Kennedy, J.D., and Seyal, M. (2017). Potentially high-risk cardiac arrhythmias with focal to bilateral tonic-clonic seizures and generalized tonic-clonic seizures are associated with the duration of periictal hypoxemia. Epilepsia *58*, 2164–2171. https://doi.org/10.1111/epi.13934.
5. Hesdorffer, D.C., Tomson, T., Benn, E., Sander, J.W., Nilsson, L., Langan, Y., Walczak, T.S., Beghi, E., Brodie, M.J., and Hauser, A.; ILAE Commission on Epidemiology; Subcommission on Mortality (2011). Combined analysis of risk factors for SUDEP. Epilepsia *52*, 1150–1159. https://doi.org/10.1111/j.1528-1167.2010.02952.x.
6. Bone, B., Fogarasi, A., Schulz, R., Gyimesi, C., Kalmar, Z., Kovacs, N., Ebner, A., and Janszky, J. (2012). Secondarily generalized seizures in

temporal lobe epilepsy. Epilepsia *53*, 817–824. https://doi.org/10.1111/j.1528-1167.2012.03435.x.

7. Jallon, P., and Latour, P. (2005). Epidemiology of idiopathic generalized epilepsies. Epilepsia *46* (*Suppl 9*), 10–14. https://doi.org/10.1111/j.1528-1167.2005.00309.x.
8. Miyazaki, T., Abe, H., Uchida, H., and Takahashi, T. (2021). Translational medicine of the glutamate AMPA receptor. Proc. Jpn. Acad. Ser. B Phys. Biol. Sci. *97*, 1–21. https://doi.org/10.2183/pjab.97.001.
9. Andrade-Machado, R., Benjumea Cuartas, V., and Muhammad, I.K. (2021). Recognition of interictal and ictal discharges on EEG. Focal vs generalized epilepsy. Epilepsy Behav. *117*, 107830. https://doi.org/10.1016/j.yebeh.2021.107830.
10. Pitkänen, A., Löscher, W., Vezzani, A., Becker, A.J., Simonato, M., Lukasiuk, K., Gröhn, O., Bankstahl, J.P., Friedman, A., Aronica, E., et al. (2016). Advances in the development of biomarkers for epilepsy. Lancet Neurol. *15*, 843–856. https://doi.org/10.1016/s1474-4422(16)00112-5.
11. Sarikaya, I. (2015). PET studies in epilepsy. Am. J. Nucl. Med. Mol. Imaging *5*, 416–430.
12. Turrigiano, G.G., and Nelson, S.B. (2000). Hebb and homeostasis in neuronal plasticity. Curr. Opin. Neurobiol. *10*, 358–364. https://doi.org/10.1016/s0959-4388(00)00091-x.
13. Malenka, R.C., and Bear, M.F. (2004). LTP and LTD: an embarrassment of riches. Neuron *44*, 5–21.
14. Lüscher, C., and Malenka, R.C. (2012). NMDA receptor-dependent long-term potentiation and long-term depression (LTP/LTD). Cold Spring Harb. Perspect. Biol. *4*, a005710. https://doi.org/10.1101/cshperspect.a005710.
15. Fox, K., and Stryker, M. (2017). Integrating Hebbian and homeostatic plasticity: introduction. Philos. Trans. R. Soc. Lond. B Biol. Sci. *372*, 20160413. https://doi.org/10.1098/rstb.2016.0413.
16. Turrigiano, G.G. (1999). Homeostatic plasticity in neuronal networks: the more things change, the more they stay the same. Trends Neurosci. *22*, 221–227. https://doi.org/10.1016/s0166-2236(98)01341-1.
17. Fernandes, D., and Carvalho, A.L. (2016). Mechanisms of homeostatic plasticity in the excitatory synapse. J. Neurochem. *139*, 973–996. https://doi.org/10.1111/jnc.13687.
18. Huganir, R.L., and Nicoll, R.A. (2013). AMPARs and synaptic plasticity: the last 25 years. Neuron *80*, 704–717. https://doi.org/10.1016/j.neuron.2013.10.025.
19. Malenka, R.C. (2003). Synaptic plasticity and AMPA receptor trafficking. Ann. N. Y. Acad. Sci. *1003*, 1–11.
20. Malinow, R., and Malenka, R.C. (2002). AMPA receptor trafficking and synaptic plasticity. Annu. Rev. Neurosci. *25*, 103–126.
21. Kessels, H.W., and Malinow, R. (2009). Synaptic AMPA receptor plasticity and behavior. Neuron *61*, 340–350.
22. Derkach, V.A., Oh, M.C., Guire, E.S., and Soderling, T.R. (2007). Regulatory mechanisms of AMPA receptors in synaptic plasticity. Nat. Rev. Neurosci. *8*, 101–113.
23. Jitsuki, S., Takemoto, K., Kawasaki, T., Tada, H., Takahashi, A., Becamel, C., Sano, A., Yuzaki, M., Zukin, R.S., Ziff, E.B., et al. (2011). Serotonin mediates cross-modal reorganization of cortical circuits. Neuron *69*, 780–792.
24. Mitsushima, D., Ishihara, K., Sano, A., Kessels, H.W., and Takahashi, T. (2011). Contextual learning requires synaptic AMPA receptor delivery in the hippocampus. Proc. Natl. Acad. Sci. USA *108*, 12503–12508. https://doi.org/10.1073/pnas.1104558108.
25. Mitsushima, D., Sano, A., and Takahashi, T. (2013). A cholinergic trigger drives learning-induced plasticity at hippocampal synapses. Nat. Commun. *4*, 2760. https://doi.org/10.1038/ncomms3760.
26. Takemoto, K., Iwanari, H., Tada, H., Suyama, K., Sano, A., Nagai, T., Hamakubo, T., and Takahashi, T. (2017). Optical inactivation of synaptic AMPA receptors erases fear memory. Nat. Biotechnol. *35*, 38–47. https://doi.org/10.1038/nbt.3710.
27. Takahashi, T., Svoboda, K., and Malinow, R. (2003). Experience strengthening transmission by driving AMPA receptors into synapses. Science *299*, 1585–1588.
28. Abe, H., Jitsuki, S., Nakajima, W., Murata, Y., Jitsuki-Takahashi, A., Katsuno, Y., Tada, H., Sano, A., Suyama, K., Mochizuki, N., et al. (2018). CRMP2-binding compound, edonerpic maleate, accelerates motor function recovery from brain damage. Science *360*, 50–57. https://doi.org/10.1126/science.aao2300.
29. Turrigiano, G.G., Leslie, K.R., Desai, N.S., Rutherford, L.C., and Nelson, S.B. (1998). Activity-dependent scaling of quantal amplitude in neocortical neurons. Nature *391*, 892–896. https://doi.org/10.1038/36103.
30. Scharfman, H.E. (2002). Epilepsy as an example of neural plasticity. Neuroscientist *8*, 154–173. https://doi.org/10.1177/107385840200800211.
31. Zilles, K., Qu, M.S., Köhling, R., and Speckmann, E.J. (1999). Ionotropic glutamate and GABA receptors in human epileptic neocortical tissue: quantitative in vitro receptor autoradiography. Neuroscience *94*, 1051–1061.
32. French, J.A., Krauss, G.L., Wechsler, R.T., Wang, X.F., DiVentura, B., Brandt, C., Trinka, E., O'Brien, T.J., Laurenza, A., Patten, A., and Bibbiani, F. (2015). Perampanel for tonic-clonic seizures in idiopathic generalized epilepsy A randomized trial. Neurology *85*, 950–957. https://doi.org/10.1212/wnl.0000000000001930.
33. Krauss, G.L., Serratosa, J.M., Villanueva, V., Endziniene, M., Hong, Z., French, J., Yang, H., Squillacote, D., Edwards, H.B., Zhu, J., and Laurenza, A. (2012). Randomized phase III study 306: adjunctive perampanel for refractory partial-onset seizures. Neurology *78*, 1408–1415. https://doi.org/10.1212/WNL.0b013e318254473a.
34. Miyazaki, T., Nakajima, W., Hatano, M., Shibata, Y., Kuroki, Y., Arisawa, T., Serizawa, A., Sano, A., Kogami, S., Yamanoue, T., et al. (2020). Visualization of AMPA receptors in living human brain with positron emission tomography. Nat. Med. *26*, 281–288. https://doi.org/10.1038/s41591-019-0723-9.
35. Miyazaki, T., Takayama, Y., Iwasaki, M., Hatano, M., Nakajima, W., Ikegaya, N., Yamamoto, T., Tsuchimoto, S., Kato, H., and Takahashi, T. (2022). Epileptic discharges initiate from brain areas with elevated accumulation of alpha-amino-3-hydroxy-5-methyl-4-isoxazole propionic acid receptors. Brain Commun. *4*, fcac023. https://doi.org/10.1093/braincomms/fcac023.
36. Hatano, M., Miyazaki, T., Ishiwata, Y., Nakajima, W., Arisawa, T., Kuroki, Y., Kobayashi, A., Takada, Y., Ogawa, M., Kawamura, K., et al. (2021). Biodistribution and radiation dosimetry of the positron emission tomography probe for AMPA receptor, [(11)C]K-2, in healthy human subjects. Sci. Rep. *11*, 1598. https://doi.org/10.1038/s41598-021-81002-3.
37. Arisawa, T., Miyazaki, T., Ota, W., Sano, A., Suyama, K., Takada, Y., and Takahashi, T. (2021). [(11)C]K-2 image with positron emission tomography represents cell surface AMPA receptors. Neurosci. Res. *173*, 106–113. https://doi.org/10.1016/j.neures.2021.05.009.
38. Alvarado-Rojas, C., Lehongre, K., Bagdasaryan, J., Bragin, A., Staba, R., Engel, J., Jr., Navarro, V., and Le Van Quyen, M. (2013). Single-unit activities during epileptic discharges in the human hippocampal formation. Front. Comput. Neurosci. *7*, 140. https://doi.org/10.3389/fncom.2013.00140.
39. Benedek, K., Berényi, A., Gombkötő, P., Piilgaard, H., and Lauritzen, M. (2016). Neocortical gamma oscillations in idiopathic generalized epilepsy. Epilepsia *57*, 796–804. https://doi.org/10.1111/epi.13355.
40. Fuchs, E.C., Zivkovic, A.R., Cunningham, M.O., Middleton, S., Lebeau, F.E.N., Bannerman, D.M., Rozov, A., Whittington, M.A., Traub, R.D., Rawlins, J.N.P., and Monyer, H. (2007). Recruitment of parvalbumin-positive interneurons determines hippocampal function and associated behavior. Neuron *53*, 591–604. https://doi.org/10.1016/j.neuron.2007.01.031.
41. Lundstrom, B.N., Boly, M., Duckrow, R., Zaveri, H.P., and Blumenfeld, H. (2019). Slowing less than 1 Hz is decreased near the seizure onset zone. Sci. Rep. *9*, 6218. https://doi.org/10.1038/s41598-019-42347-y.
42. Ren, L., Kucewicz, M.T., Cimbalnik, J., Matsumoto, J.Y., Brinkmann, B.H., Hu, W., Marsh, W.R., Meyer, F.B., Stead, S.M., and Worrell, G.A. (2015). Gamma oscillations precede interictal epileptiform spikes in the seizure

onset zone. Neurology *84*, 602–608. https://doi.org/10.1212/wnl.0000000000001234.

43. Innis, R.B., Cunningham, V.J., Delforge, J., Fujita, M., Gjedde, A., Gunn, R.N., Holden, J., Houle, S., Huang, S.C., Ichise, M., et al. (2007). Consensus nomenclature for in vivo imaging of reversibly binding radioligands. J. Cereb. Blood Flow Metab. *27*, 1533–1539. https://doi.org/10.1038/sj.jcbfm.9600493.
44. Hirose, S., Mitsudome, A., Okada, M., and Kaneko, S.; Epilepsy Genetic Study Group Japan (2005). Genetics of idiopathic epilepsies. Epilepsia *46* (*Suppl 1*), 38–43. https://doi.org/10.1111/j.0013-9580.2005.461011.x.
45. Gardiner, M. (2005). Genetics of idiopathic generalized epilepsies. Epilepsia *46* (*Suppl 9*), 15–20. https://doi.org/10.1111/j.1528-1167.2005.00310.x.
46. Geller, A.S., Burke, J.F., Sperling, M.R., Sharan, A.D., Litt, B., Baltuch, G.H., Lucas, T.H., 2nd, and Kahana, M.J. (2014). Eye closure causes widespread low-frequency power increase and focal gamma attenuation in the human electrocorticogram. Clin. Neurophysiol. *125*, 1764–1773. https://doi.org/10.1016/j.clinph.2014.01.021.
47. Goelz, H., Jones, R.D., and Bones, P.J. (2000). Wavelet analysis of transient biomedical signals and its application to detection of epileptiform activity in the EEG. Clin. Electroencephalogr. *31*, 181–191. https://doi.org/10.1177/155005940003100406.
48. Gallentine, W.B., and Mikati, M.A. (2012). Genetic generalized epilepsies. J. Clin. Neurophysiol. *29*, 408–419. https://doi.org/10.1097/WNP.0b013e31826bd92a.
49. Mullen, S.A., and Berkovic, S.F.; ILAE Genetics Commission (2018). Genetic generalized epilepsies. Epilepsia *59*, 1148–1153. https://doi.org/10.1111/epi.14042.
50. Loomba, S., Straehle, J., Gangadharan, V., Heike, N., Khalifa, A., Motta, A., Ju, N., Sievers, M., Gempt, J., Meyer, H.S., and Helmstaedter, M. (2022). Connectomic comparison of mouse and human cortex. Science *377*, eabo0924. https://doi.org/10.1126/science.abo0924.
51. Beghi, E., Giussani, G., and Sander, J.W. (2015). The natural history and prognosis of epilepsy. Epileptic Disord. *17*, 243–253. https://doi.org/10.1684/epd.2015.0751.
52. Fine, A., and Wirrell, E.C. (2020). Seizures in children. Pediatr. Rev. *41*, 321–347. https://doi.org/10.1542/pir.2019-0134.
53. van Ool, J.S., Snoeijen-Schouwenaars, F.M., Schelhaas, H.J., Tan, I.Y., Aldenkamp, A.P., and Hendriksen, J.G.M. (2016). A systematic review of neuropsychiatric comorbidities in patients with both epilepsy and intellectual disability. Epilepsy Behav. *60*, 130–137. https://doi.org/10.1016/j.yebeh.2016.04.018.
54. Watkins, L., O'Dwyer, M., Kerr, M., Scheepers, M., Courtenay, K., and Shankar, R. (2020). Quality improvement in the management of people with epilepsy and intellectual disability: the development of clinical guidance. Expert Opin. Pharmacother. *21*, 173–181. https://doi.org/10.1080/14656566.2019.1695780.
55. Buzsáki, G. (2002). Theta oscillations in the hippocampus. Neuron *33*, 325–340. https://doi.org/10.1016/s0896-6273(02)00586-x.
56. Buzsàki, G., and Eidelberg, E. (1983). Phase relations of hippocampal projection cells and interneurons to theta activity in the anesthetized rat. Brain Res. *266*, 334–339. https://doi.org/10.1016/0006-8993(83)90665-0.
57. Nuñez, A., and Buño, W. (2021). The theta rhythm of the Hippocampus: from neuronal and circuit mechanisms to behavior. Front. Cell. Neurosci. *15*, 649262. https://doi.org/10.3389/fncel.2021.649262.
58. Stark, E., Eichler, R., Roux, L., Fujisawa, S., Rotstein, H.G., and Buzsáki, G. (2013). Inhibition-induced theta resonance in cortical circuits. Neuron *80*, 1263–1276. https://doi.org/10.1016/j.neuron.2013.09.033.
59. Scheffer, I.E., Berkovic, S., Capovilla, G., Connolly, M.B., French, J., Guilhoto, L., Hirsch, E., Jain, S., Mathern, G.W., Moshé, S.L., et al. (2017). ILAE classification of the epilepsies: position paper of the ILAE commission for classification and terminology. Epilepsia *58*, 512–521. https://doi.org/10.1111/epi.13709.
60. WorldHealthOrganization (1992). The ICD-10 Classification of Mental and Behavioural Disorders : Clinical Descriptions and Diagnostic Guidelines (World Health Organization).
61. AmericanPsychiatricAssociation (2013). Diagnostic and Statistical Manual of Mental Disorders, 5th Ed.
62. Okazawa, H., Ikawa, M., Jung, M., Maruyama, R., Tsujikawa, T., Mori, T., Rahman, M.G.M., Makino, A., Kiyono, Y., and Kosaka, H. (2020). Multimodal analysis using [(11)C]PiB-PET/MRI for functional evaluation of patients with Alzheimer's disease. EJNMMI Res. *10*, 30. https://doi.org/10.1186/s13550-020-00619-z.
63. Logan, J., Fowler, J.S., Volkow, N.D., Wang, G.J., Ding, Y.S., and Alexoff, D.L. (1996). Distribution volume ratios without blood sampling from graphical analysis of PET data. J. Cereb. Blood Flow Metab. *16*, 834–840. https://doi.org/10.1097/00004647-199609000-00008.
64. Kimura, Y., Naganawa, M., Shidahara, M., Ikoma, Y., and Watabe, H. (2007). PET kinetic analysis –pitfalls and a solution for the Logan plot. Ann. Nucl. Med. *21*, 1–8. https://doi.org/10.1007/bf03033993.
65. Ashburner, J., and Friston, K.J. (2005). Unified segmentation. Neuroimage *26*, 839–851. https://doi.org/10.1016/j.neuroimage.2005.02.018.
66. Ashburner, J. (2007). A fast diffeomorphic image registration algorithm. Neuroimage *38*, 95–113. https://doi.org/10.1016/j.neuroimage.2007.07.007.

STAR★METHODS

KEY RESOURCES TABLE

REAGENT or RESOURCE	SOURCE	IDENTIFIER
Software and algorithms		
PMOD PNEURO tool version 3.709	PMOD Technologies	https://www.pmod.jp/
R version 4.0.0	R Core Team	https://www.r-project.org/
SPM12	SPM	https://www.fil.ion.ucl.ac.uk/spm/software/spm12/

RESOURCE AVAILABILITY

Lead contact

Further information and requests for resources should be directed to and will be fulfilled by the lead contact, Takuya,Takahashi(takahast@yokohama-cu.ac.jp).

Materials availability

The study did not generate new unique reagents.

Data and code availability

All requests for raw and analyzed data were reviewed promptly by Yokohama City University Research. The promotion department determines whether the request is subject to any intellectual property or confidentiality obligations and is further inspected by the institutional review board of Yokohama City University Hospital. Based on these approaches, the derived data will be released via material transfer agreement from the corresponding author. All data reported in this paper will be shared by the lead contact upon request.

Any additional information required to reanalyze the data reported in this work paper is available from the lead contact upon request.

This paper does not report the original code

EXPERIMENTAL MODEL AND SUBJECT DETAILS

Ethics statement

This clinical study was performed under protocols approved by the Yokohama City University Human Investigation Committee in accordance with the ethical guidelines for medical and health research involving human participants drawn up by the Japan Ministry of Health, Labor, and Welfare (trial registry number jRCT1030220299). This study was composed of three independent clinical trials that have already completed patient or healthy control enrollment (two trials for epilepsy and one trial for healthy subjects). Data were analyzed comprehensively in this study to elucidate the biological characteristics of four seizure types i.e., focal onset seizure without generalized seizure, FBTCS, focal onset seizure (including focal onset seizure without generalized seizure and FBTCS), and generalized onset seizure. The inclusion criteria were as follows: (1) male individuals in their 20-49 years old whose [^{11}C]K-2 data were obtained from the jRCTs031200083 trial; (2) male individuals whose [^{11}C]K-2 and scalp-EEG data were obtained from the UMIN000025132 trial; and (3) male individuals whose [^{11}C]K-2 and scalp-EEG data were obtained from the UMIN000031624 trial. The exclusion criteria were as follows: (1) patients with epilepsy who did not have seizures for 1 year prior to the [^{11}C]K-2 PET scan, (2) patients with epilepsy whose EEGs under resting closed-eye conditions were recorded for less than 1 min; and (3) patients with epilepsy whose seizure types could not be classified by their histories. All participants provided written informed consent after receiving detailed information about the study protocol.

Human participants

This study was composed of three clinical trials involving patients with epilepsy and healthy controls.

Clinical trial 1 for patients with epilepsy

A clinical trial (trial registry number was UMIN000031624) with the title ‘‘The clinical trial to examine the densities of AMPA receptors in epilepsy patients with [^{11}C]K-2’’ was carried out to examine the differences in the distributions of AMPARs among the groups divided by seizure pattern in comparison with those of healthy controls. The date of the first treatment was August 27, 2018 and that of the last treatment was August 3, 2020. Patients who met the following criteria were included in the study: (1) being diagnosed with epilepsy on

the basis of the International League Against Epilepsy (ILAE) criteria,[59] (2) having seizures 12 months prior to registration, (3) no history of neurosurgery, (4) ages of 20-59 years, and (5) being capable of providing informed consent. Patients were excluded if they met any of the following criteria: (1) having experienced electric stimulation therapy, (2) having severe renal dysfunction (serum creatinine > 1.5 mg/dL), (3) having severe liver dysfunction (serum AST and ALT > 150 IU/L), (4) having severe cardiovascular disorder, (5) having tattoos, (6) having claustrophobia, (7) being unable to agree to use contraception within 7 days of [^{11}C]K-2 PET imaging , (8) taking perampanel or topiramate within 1 month before the trial registration, (9) undergoing nuclear medicine examination within 1 week before this registration, (10) participating in other clinical trials using unapproved nuclear medicine examination within 6 months before this registration, (11) participating in other clinical trials within 12 weeks before this registration, and (12) being deemed by doctors to be inappropriate for other reasons. Finally, 33 patients met the eligibility criteria and were registered for the trial (all males; 33.6 ± 10.0 years of age). These patients were scheduled to undergo scalp EEG, MRI, and PET scans with [^{11}C]K-2, which were performed at the Yokohama City University Hospital, Keio University Hospital, or Fukushima Medical University Hospital**.** A total of five patients were excluded from the analysis for the following reasons: one patient complained of mood discomfort during PET imaging, two patients had severe status epilepticus immediately prior to the PET scan, and two patients had excessive head movements during PET imaging.

Clinical trial 2 for patients with epilepsy

The other clinical trial (trial registry number UMIN000025132) with the title "The clinical pilot study to examine the distribution of [^{11}C]K-2 in depression, bipolar disease, schizophrenia, addiction, ASD, epilepsy, and FTD patients in order to develop the novel diagnostic method in cross-sectional way toward these diseases." The date of the first treatment was November 20, 2016, and that of the last treatment was December 28, 2020. The trial was carried out to explore specific brain regions which differed with respect to accumulation of [^{11}C]K-2 for each disease such as depression, bipolar disease, schizophrenia, addiction, ASD, epilepsy, and FTD and healthy controls. Patients who met the following criteria were included in the study: (1) being diagnosed with epilepsy using International Classification of Diseases (ICD-10) and ILAE definition,[59,60] (2) male individuals at the ages of 30–49 years, and (3) being capable of providing informed consent. Subjects excluded from the study if they met any of the following criteria: (1) undergoing hemodialysis, (2) having severe liver dysfunction, (3) having neurological disorders except for neurodegenerative diseases and stroke, (5) were consuming perampanel, (6) having a history of substance abuse, (7) a positive result in a urine screening test for addictive substances, (8) using addictive substances within the past 2 weeks, (9) having experienced any of the following neuromodulation therapies: repetitive transcranial magnetic stimulation, deep brain stimulation, transcranial direct current stimulation), and multiple subpial transection, (10) having metals or a pacemaker inside their body, (11) having a large head, neck, or body which did not allow them to fit in an MRI scanner, (12) having tattoos, (13) having claustrophobia, (14) having significant abnormalities in the brain, (15) showing serum Creatinine > 1.5 mg/dL or serum aspartate aminotransferase (AST) and alanine transaminase (ALT) > 100 IU/L, (16) having undergone any examination with unapproved nuclear medicine in clinical trials within the past 6 months before this registration, (17) participating in other clinical trials within the past 12 weeks before this registration, or (18) being deemed by doctors to be inappropriate for other reasons. Regarding patients with epilepsy, 10 patients met the eligibility criteria and were registered (all males; 39.4 ± 6.87 years of age). These patients underwent scalp EEG, MRI, and PET with [^{11}C]K-2, which was performed at the Yokohama City University Hospital.

Clinical trials with healthy controls

A clinical trial (trial registry number jRCTs031200083) with the title "A clinical trial to examine age-and-sex-related changes in AMPA receptor density in healthy volunteers." The date of the first treatment was October 9, 2020, and that of the last treatment was March 7, 2022. The trial was carried out to determine whether AMPA receptor density changes with age and sex in healthy controls. Healthy individuals who met the following criteria were included in the study: (1) male individuals at the age of 20–49 years at the time of obtaining informed consent, (2) having no history of mental or neurological disease, (3) having sufficient judgment ability to provide consent as per the evaluation by MacArthur Competence Assessment Tool for Treatment, and (4) having no current mental disorders based on any criteria in the Structured Clinical Interview for Diagnostic and Statistical Manual of Mental Disorders, DSM-5, and ICD-10.[60,61] Subjects who were excluded met the following criteria: (1) taking psychotropic, antidepressant, hypnotic, anxiolytic, or antipsychotic drugs, (2) being pregnant or lactating, (3) being hypersensitive to ethanol, (4) having neurological diseases (neurodegenerative disease, minor cerebral hemorrhage or cerebral infarction), (5) having a history of malignant brain tumor, (6) having a history of epilepsy, (7) receiving medical treatment for other diseases, (8) having substance-related disorders except for nicotine and caffeine within 6 months from this registration, (9) a positive result for urine screening for recreational drugs, (10) having a pacemaker or any other metal devices in the body, (11) having a large head, neck, and body size for MRI scanner, (12) having tattoos on their skin, (13) having severe claustrophobia, (14) having congenital or traumatic brain abnormalities, (15) showing serum Creatinine > 1.5 mg/dL or serum AST and ALT > 150 IU/L, (16) having undergone [^{11}C] K-2 PET in other clinical trials, (17) participating in unapproved nuclear medicine tests or other clinical trials within 6 months before registration, (18) participating in other clinical trials within 12 weeks prior to enrollment (limited to those with invasion/intervention) or other clinical trials, (19) being deemed by the investigator to be inappropriate for other reasons. A total of 33 healthy controls met the eligibility criteria and were registered (33 males; 33.52 ± 8.85 years of age). Each participant underwent an MRI scan and a PET scan with [^{11}C]K-2, which was performed at the Yokohama City University Hospital, Kyushu University Hospital or University of Fukui Hospital. Two healthy controls were excluded from the analysis for the following reasons: one could not undergo PET scan due to failure in synthesis of the PET compound, and one was found to have a history of epilepsy after registration.

Scalp-electroencephalogram

Resting, wakeful, and interictal scalp EEG were recorded for each subject while the participants were seated comfortably with their eyes closed. A Neurofax EEG-1524Ver.05-74 system (Nihon Kohden Corp., Tokyo, Japan) was used at the Yokohama City University Hospital for 17 patients.

For four patients at the Fukushima Medical University Hospital, a Neuro fax EEG-1200 Ver.05-04 system (Nihon Kohden corp., Tokyo, Japan) was used. EEG data at both facilities were recorded using 19 electrodes according to the international 10-20 system at a sampling rate of 500 Hz, and the impedance levels were set to less than 10 kΩ.

For nine patients at Keio University Hospital, EEG was recorded with a TruScan EEG system (Deymed Diagnostic s.r.o., Hronov, Czech) at a sampling rate of 3000 Hz using a 62-channel electrode cap. The impedance levels were set at less than 5 kΩ, and the data from 19 electrodes corresponding to the international 10-20 system were used for analysis.

All data processing was performed using house-made programs in R (version 4.0.0,R Core Team,2021). The recorded resting EEG was visually checked, and a wakeful period of 1–5 min without paroxysmal activities was extracted for analysis. The signals were band-pass filtered between 1–100 Hz. Blink, eye movement, and muscular artifacts were removed using independent component analysis. The signal was then divided into delta (1-3 Hz), theta (4-7 Hz), alpha (8-13 Hz), beta (14-29 Hz), and gamma (30-70 Hz) frequency ranges using Butterworth bandpass filters. The root-mean-square amplitude was calculated for each frequency band.

In vivo PET and MRI imaging

[^{11}C]K-2 was synthesized in accordance with GMP ordinance and was certified by the Japanese Society of Nuclear Medicine.

Yokohama City University Hospital

PET scans were performed using a Toshiba Aquiduo scanner (TOSHIBA Medical, Gunma,324-8550,Japan) and Celesteion PCA-9000A/2A (Canon Medical, Gunma,324-8550,Japan). Aquiduo provided an axial field of view (FOV) of 240 mm and 80 contiguous 2.0 mm thick slices. A 4.7 s transmission scan was performed for attenuation correction (AC), and a 60 s intravenous injection of [^{11}C]K-2 (375 ± 8.4 MBq) was administered, followed by an emission scan for 60 min with frames of 18 × 10 s, 2 × 30 s, 7 × 60 s, 1 × 2 min, 1 × 3 min, 3 × 5 min, and 3 × 10 min. Dynamic images were reconstructed with 2D-OSEM using four iterations, 14 subsets, a 128 matrix, a zoom of 2.8, and a 5.0 mm Gaussian filter. Celesteion provided an axial FOV of 240 mm and 96 contiguous 2.0 mm thick slices. A 15.2 s transmission scan was performed for attenuation correction (AC), and a 60 s intravenous injection of [^{11}C]K-2 (376.2 ± 10.1 MBq) was administered, followed by an emission scan of 60 min with 35 frames. Dynamic images were reconstructed with TOF 3D-OSEM using two iterations, 20 subsets, 128 matrix, zoom factor 1.0, and 5.0 mm Gaussian filter. Each participant underwent MRI using a GE DISCOVERY MR750 (General Electric Medical Systems). 3D-T1-weighted (T1WI) anatomical MRI scans were acquired using the following parameters: voxel size = 0.9 × 0.9 × 0.9 mm, repetition time (TR) / time to echo (TE) = 7.016/3.056 ms, flip angle (FA) = 8°, FOV = 220 mm, matrix = 256 × 256.

Keio University Hospital

PET scans were performed with a Biograph mCT Flow (Siemens Medical Solutions USA), which provided an axial FOV of 300 mm and 111 contiguous 2.0 mm-thick slices. A 6.56 s transmission scan was performed for AC, and a 60 s intravenous injection of [^{11}C]K-2 (367.8 ± 9.5 MBq) was administered, followed by an emission scan of 60 min with 35 frames. Dynamic images were reconstructed with 3D-OSEM using four iterations, 24 subsets, a 200 matrix, a zoom factor 2.0, and a 3.0 mm Gaussian filter. Each participant underwent MRI with the 3D MPRAGE protocol on a MAGNETOM Prisma (SIEMENS Healthineers) at the University of Tokyo. 3D-T1WI images were acquired using the following parameters: voxel size = 0.8 × 0.8 × 0.8 mm, TR/TE = 2400/2.22 ms, FA = 8°, FOV = 208 mm, matrix = 300 × 320.

Fukushima Medical University

PET scans were performed with a Biograph mCT (Siemens Healthcare), which provided an axial FOV of 221 mm and 148 contiguous 3.0 mm-thick slices. A transmission scan was performed for AC, and a 60 sec intravenous injection of [^{11}C]K-2 (378 ± 5.5 MBq) was administered, followed by an emission scan of 60 min with frames of 18 × 10 s, 2 × 30s, 7 × 60 s, 1 × 2 min, 1 × 3 min, 3 × 5 min, and 3 × 10 min. Dynamic images were reconstructed with TOF 3D-OSEM using five iterations, 21 subsets, a 400 matrix, a zoom of 2.0, and a 2.0 mm Gaussian filter. Each subject underwent MRI with the 3D MPRAGE protocol on a Biograph mMR (SIEMENS Healthineers). 3D-T1WI images were acquired using the following parameters: voxel size = 0.9 × 0.9 × 0.9 mm, TR/TE = 1900/3.08 ms, FA = 9°, FOV = 192 mm, matrix = 265 × 265.

Kyushu university hospital

PET scans were performed using a Biograph Vision (Siemens Healthcare) and a Biograph mCT scanner (Siemens Healthcare). Vison provided an axial FOV of 357 mm and 263 contiguous 1.0 mm-thick slices. A 26.67 s transmission scan was performed for AC, and a 60 s intravenous injection of [^{11}C]K-2 (385.3 ± 2.0 MBq) was administered, followed by an emission scan of 60 min with 35 frames. Dynamic images were reconstructed with a 3D-OSEM + TOF using eight iterations, five subsets, and a 5.0 mm Gaussian filter. mCT provided an axial FOV of 250 mm and 165 contiguous 1.0 mm-thick slices. A 9.38 s transmission scan was performed for AC, and a 60 s intravenous injection of [^{11}C]K-2 (388.8 MBq) was administered, followed by an emission scan of 60 min with 35 frames. Dynamic images were reconstructed with 3D-OSEM + TOF using five iterations, 21 subsets, and a 5.0 mm Gaussian filter. Each participant underwent MRI with the 3D MPRAGE protocol on an Ingenia 3.0 T scanner (Phillips). 3D-T1WI images were acquired using the following parameters: voxel size = 1.2 × 1.0 × 1.0 mm, TR/TE = 6.8/3.1 ms, FA = 9°, FOV = 170 mm, matrix = 256 × 256.

University of Fukui Hospital

PET and MRI were performed with Signa PET/MRI (GE Healthcare) for simultaneous PET and MRI acquisition. During the PET scan, a 60 sec intravenous injection of [^{11}C]K-2 (355.5 ± 14.8 MBq) was administered, followed by an emission scan of 60 min with 35 frames, and a 3D radial MR acquisition for the zero-echo time (ZTE) method in the axial direction was performed for AC of PET data with the following parameters: FOV 256 mm, 89 contiguous 2.78 mm thick slices, bandwidth ± 62.5 kHz, and acquisition time of 41 s. In the ZTE-AC method, the following process was used to create the MR-AC map based on a previous study.[62]

Dynamic images were reconstructed with 3D-OSEM + TOF using three iterations, 28 subsets, a 128 matrix, and a 5.0 mm Gaussian filter. High resolution 3D-T1WI were acquired using the following sequence: voxel size = 0.9 × 0.9 × 0.9 mm, TR/TE = 8.5/3.3 ms, FA = 8°, FOV = 196 mm, Matrix = 256 × 256.

METHOD DETAILS

Acquisition of tissue time activity curve

For each participant, PET and T1WI images were normalized to the MNI (Montreal Neurological Institute) standard space. The PMOD PNEURO tool version 3.709 (PMOD Technologies) was used for normalization. The volume of interest (VOI) of the white matter (WM) that was used as the reference region was calculated using SPM 8. It was obtained by satisfying the following conditions for voxel values: the probability of presence of WM >0.9, the 8 mm-smoothed grey matter (GM) <0.05, and the 8 mm-smoothed cerebrospinal fluid (CSF) <0.05 using SPM 8.[34] Time-activity curves (TACs) were created using the VOI of these brain regions. The standardized uptake value (SUV) for each brain region was calculated as the radioactivity concentration in the region at time t (Bq ml^{-1})/(injected dose (Bq)/body weight [kg]).

Logan graphical analysis

We applied the binding potential to a reference region, non-displaceable binding potential (BP_{ND}), to quantify the receptor density of AMPAR. BP_{ND} is defined as the ratio of the receptor density to the disassociation rate of K-2 and AMPAR compounds; therefore, it is proportional to the density of receptor.[43] We computed BP_{ND} using the Logan Graphical Analysis (LGA) method with a reference region and without the clearance rate of K-2 in the reference region, where BP_{ND} could be estimated using a linear regression.[63] The beginning of the linear regression, t*, was 20 min after the administration of K-2, and the white matter was utilized as the reference region.[34,64] All cases except one contained five data points for the regression—one case had only two points due to head movement. We could not derive statistically reliable estimates; therefore, we excluded this case.

PET and MRI imaging procedure

Summed images of [^{11}C]K-2 PET–30-50 min after the radiotracer injection were obtained for all the participants. $SUVR_{30\text{-}50\ min}$ images were obtained by dividing the value of the WM as a reference region. $SUVR_{30\text{-}50\ min}$ images were co-registered with the T1WI images using SPM 12. In 31 healthy controls and 21 patients with epilepsy, T1WI images were segmented into probability maps of GM, WM, and CSF using a unified framework for tissue segmentation.[65] Owing to artifacts at the bottom of the frontal lobe, multispectral segmentation was performed using T1- and T2-weighted MRI in nine patients with epilepsy. The DARTEL algorithm was then applied to the segmented GM and WM images to calculate the spatial transformation required for transforming each individual image into a study population template.[66] The transformation was then applied to individual $SUVR_{30\text{-}50\ min}$ images with additive linear transformation from the study population template to the MNI standard space. The spatially normalized images were then processed with an 8 mm full width-half maximum (FWHM) Gaussian filter.

Imaging data analysis

To eliminate inter-subject variation and noise from outside the brain, an explicit mask was applied before the statistical analysis. Mask image was composed of a region containing GM with a probability of 10% or more equipped in SPM12.

QUANTIFICATION AND STATICAL ANALYSIS

Correlation between $SUVR_{30\text{-}50}$ min and EEG amplitude

The correlation between $SUVR_{30\text{-}50}$ min values and the amplitudes of the gamma/theta activity in each electrode site was assessed using multiple regression analysis for four groups (1. focal onset seizure without generalized seizure, 2. FBTCS, 3. focal onset seizure (including focal onset seizure without generalized seizure and FBTCS), and 4. generalized onset seizure). Statistical significance was set at $p < 0.05$ (peak-level uncorrected), and the false discovery rate (FDR) was corrected at $p < 0.05$ (cluster-level inference) for multiple comparisons across all in-mask voxels. Peak-level uncorrected P-value was noted in figure legend. Figure panels are composed of consecutive six pictures in each plane (axial, coronal and sagittal) and anatomical positions of six pictures are same in all figure panels.

The correlation coefficient of the scatter plots between amplitude and $SUVR_{30\text{-}50\ min}$ in clusters by SPM analysis was calculated. To determine whether the samples showed normal distribution, the Shapiro-Wilk normality test was performed, and correlations were calculated by Pearson correlation analysis for normal distribution and by Spearman correlation analysis for non-normal distribution, respectively.

Comparison of $SUVR_{30\text{-}50}$ min values between healthy controls and patients with epilepsy

Comparison of $SUVR_{30\text{-}50\ min}$ values between healthy controls and patients with epilepsy was performed using a two-sample t-test for four groups (1. focal onset seizure without generalized seizure, 2. FBTCS, 3. focal onset seizure (including focal onset seizure without generalized seizure and FBTCS), and 4. generalized onset seizure). Statistical significance was set at $p < 0.05$ (peak-level uncorrected), and the false discovery rate (FDR) was corrected at $p < 0.05$ (cluster-level inference) for multiple comparisons across all in-mask voxels. Peak-level uncorrected P-value was noted in figure legend. Figure panels are composed of consecutive six pictures in each plane (axial, coronal and sagittal) and anatomical positions of six pictures are same in all figure panels.

Elucidation of physiological fraction of AMPARs in patients with focal onset seizures

To compare gamma activity amplitude-adjusted [^{11}C]K-2 $SUVR_{30–50\ min}$ values between patients with focal onset seizures and healthy controls, we performed multivariable regression analysis with [^{11}C]K-2 $SUVR_{30–50\ min}$ as the objective variable, and the medical condition (patients with focal onset seizures or healthy controls) and gamma activity amplitude as the explanatory variables. Because the gamma activity amplitude values were not measured in healthy controls, we imputed the values as 0 in the multivariable regression analysis, which was performed using R statistical software, version 4.2.0 (R Foundation for Statistical Computing, Vienna, Austria).

ADDITIONAL RESOURCES

The clinical pilot study to examine the distribution of [11C]K-2 in depression, bipolar disease, schizophrenia, addiction, ASD, epilepsy and FTD patients in order to develop the novel diagnostic method in cross-sectional way toward these diseases (registry number UMIN00002513: https://rctportal.niph.go.jp/en/detail?trial_id=UMIN000025132)

The clinical trial to examine the densities of AMPA receptors in epilepsy patients with [^{11}C]K-2 (registry number UMIN000031624: https://rctportal.niph.go.jp/en/detail?trial_id=UMIN000031624)

A clinical trial to examine age-and-sex-related changes of AMPA receptor density in healthy volunteers (registry number jRCTs031200083: https://rctportal.niph.go.jp/en/detail?trial_id=jRCTs031200083)

Cell Reports Medicine, Volume *4*

Supplemental information

Dynamics of AMPA receptors regulate epileptogenesis in patients with epilepsy

Tsuyoshi Eiro, Tomoyuki Miyazaki, Mai Hatano, Waki Nakajima, Tetsu Arisawa, Yuuki Takada, Kimito Kimura, Akane Sano, Kotaro Nakano, Takahiro Mihara, Yutaro Takayama, Naoki Ikegaya, Masaki Iwasaki, Akitoyo Hishimoto, Yoshihiro Noda, Takahiro Miyazaki, Hiroyuki Uchida, Hideaki Tani, Nobuhiro Nagai, Teruki Koizumi, Shinichiro Nakajima, Masaru Mimura, Nozomu Matsuda, Kazuaki Kanai, Kazuhiro Takahashi, Hiroshi Ito, Yoji Hirano, Yuichi Kimura, Riki Matsumoto, Akio Ikeda, and Takuya Takahashi

Patient	Gender/age,y	Onset age,y	Duration,y	Seizure type	Estimated epileptogenic focus
1	M/33	11	22	FIAS/FAS	Left temporal lobe
2	M/48	25	23	FIAS/FAS	Right temporal lobe
3	M/26	26	1	FIAS	Left temporal lobe
4	M/38	11	27	FIAS	Right temporal lobe
5	M/38	29	9	FIAS/FAS	Frontal lobe

Table S1. Patient characteristics of focal onset seizures without generalized seizure, Related to Figure 1 and 2.

FIAS: Focal impaired awareness seizure, FAS: Focal aware seizure.

Patient	Gender /age,y	Onset age,y	Duration,y	Seizure type	Estimated epileptogenic focus
6	M/25	0	25	FIAS/FAS+FBTCS	Right hypothalamus
7	M/21	13	8	FIAS+FBTCS	Left temporal lobe
8	M/50	10	40	FIAS+FBTCS	Bilateral temporal lobe
9	M/25	9	16	FAS +FBTCS	Right frontal lobe
10	M/55	53	2	FIAS+FBTCS	Right frontal lobe
11	M/35	6	29	FAS +FBTCS	Left occipital lobe
12	M/39	18	20	FIAS+FBTCS	Right frontal lobe
13	M/45	31	14	FIAS+FBTCS	Unknown
14	M/30	28	2	FIAS+FBTCS	Right temporal lobe
15	M/31	14	17	FIAS+FBTCS	Left temporal lobe
16	M/21	15	6	FAS +FBTCS	Left frontal lobe
17	M/46	4	42	FIAS+FBTCS	Unknown
18	M/30	20	10	FIAS+FBTCS	Right frontal lobe
19	M/31	11	14	FIAS+FBTCS	Left frontal lobe
20	M/50	42	8	FIAS+FBTCS	Left temporal lobe
21	M/26	20	6	FIAS+FBTCS	Left temporal lobe
22	M/47	10	37	FIAS/FAS+FBTCS	Left temporal lobe

Table S2. Patient characteristics of focal to bilateral tonic clonic seizures, Related Figure 1 and 3

FIAS: Focal impaired awareness seizure, FAS: Focal aware seizure, FBTCS: Focal to bilateral tonic clonic seizure.

Patient	Gender /age,y	Onset age,y	Duration,y	Seizure type
23	M/28	12	16	GOTC
24	M/23	14	9	GOTC
25	M/20	12	8	GOTC
26	M/29	15	14	GOTC
27	M/49	13	36	GOTC
28	M/37	24	2	GOTC
29	M/26	24	2	GOTC
30	M/29	24	5	GOTC

Table S3. Patient characteristics of generalized onset seizures, Related to Figure 4

GOTC: Generalized onset tonic clonic.

Figure S1

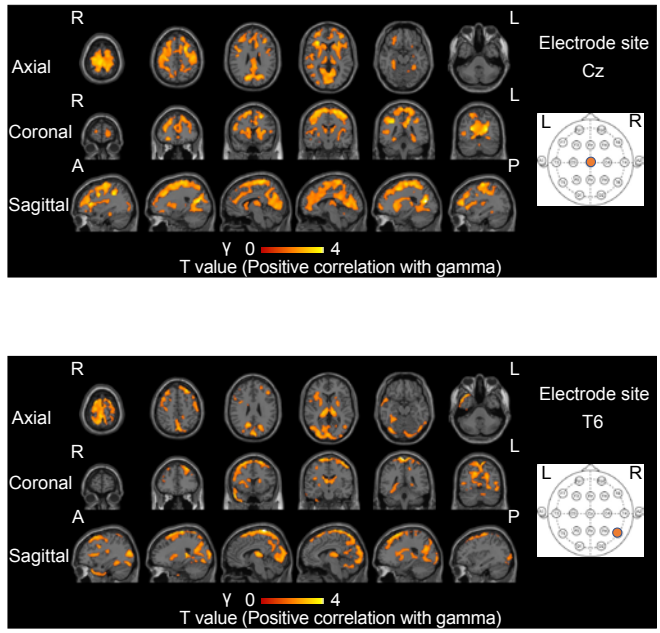

Figure S1. Positive correlation between the amount of cell surface AMPAR and the amplitude of gamma activity in focal epilepsy detected by multiple electrode sites, Related to Figure 1

SPM analysis of [^{11}C]K-2 in patients with the focal onset seizures identifies the brain regions showing a significant positive correlation between $SUVR_{30\text{-}50\ min}$ with white matter as a reference and the amplitude of gamma activity in Cz,T6 electrode site ($p < 0.05$, $T > 1.72$, one-tailed, FDRc). Scale bar indicates T value of this correlation. R: right side, L: left side, A: anterior side, P: posterior side.

FigureS2

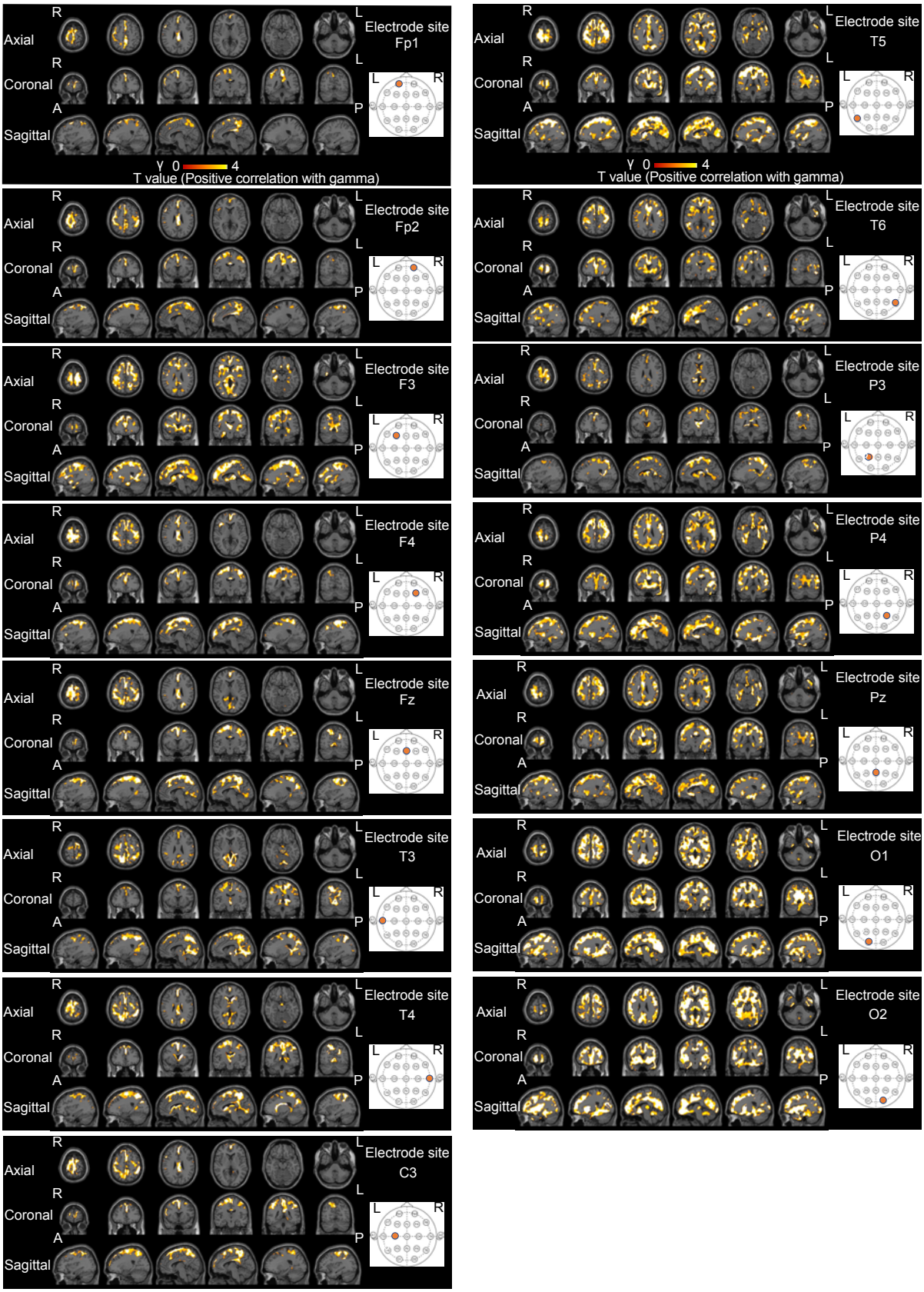
Axial
Coronal
Sagittal
R
L
A
P
Electrode site
Fp1
Fp2
F3
F4
Fz
T3
T4
C3
T5
T6
P3
P4
Pz
O1
O2
γ 0 4
T value (Positive correlation with gamma)

Figure S2. Positive AMPAR-gamma activity couplings are observed in patients with the focal onset seizures without generalized seizure detected by multiple electrode sites, Related to Figure2

SPM analysis of [^{11}C]K-2 in patients with the focal onset seizures without generalized seizure identifies the brain regions showing a significant positive correlation between $SUVR_{30\text{-}50\ min}$ with white matter as a reference and the amplitude of gamma activity in Fp1, Fp2, F3, F4, Fz, T3, T4, C3, T5, T6, P3, P4, Pz, O1, O2 electrode site ($p < 0.05$, $T > 2.35$, one-tailed, FDRc). Scale bar indicates T value of this correlation. R: right side, L: left side, A: anterior side, P: posterior side.

FigureS3

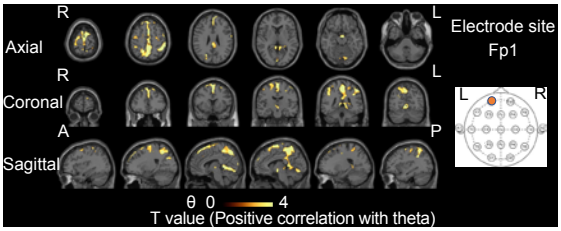
R
L
Axial
R
L
Coronal
A
P
Sagittal
Electrode site
Fp1
L
R
θ 0
4
T value (Positive correlation with theta)

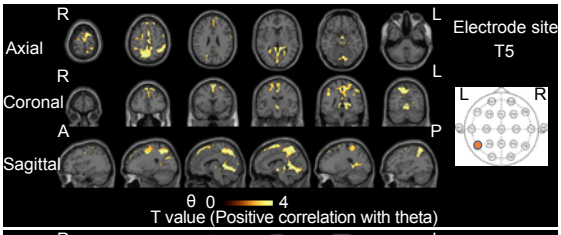
R
L
Axial
R
L
Coronal
A
P
Sagittal
Electrode site
T5
L
R
θ 0
4
T value (Positive correlation with theta)

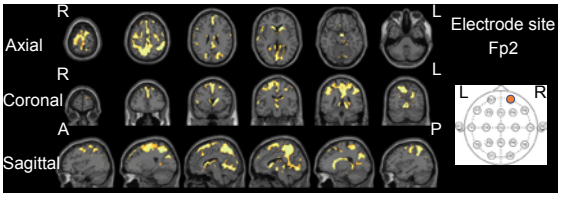
R
L
Axial
R
L
Coronal
A
P
Sagittal
Electrode site
Fp2
L
R

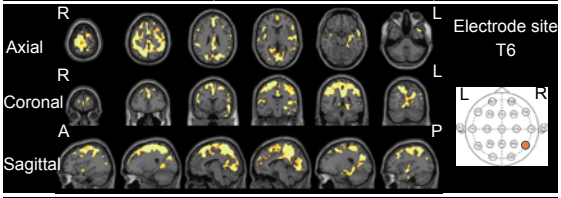
R
L
Axial
R
L
Coronal
A
P
Sagittal
Electrode site
T6
L
R

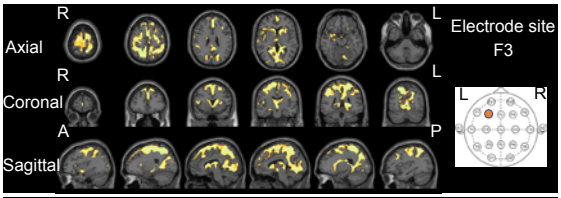
R
L
Axial
R
L
Coronal
A
P
Sagittal
Electrode site
F3
L
R

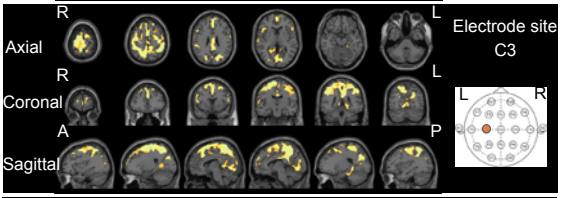
R
L
Axial
R
L
Coronal
A
P
Sagittal
Electrode site
C3
L
R

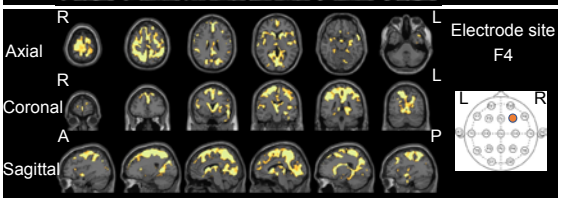
R
L
Axial
R
L
Coronal
A
P
Sagittal
Electrode site
F4
L
R

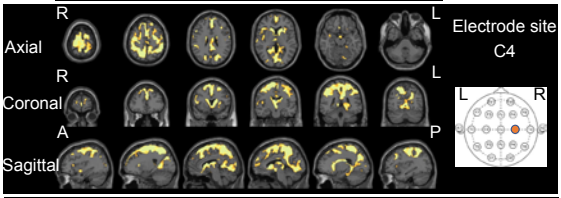
R
L
Axial
R
L
Coronal
A
P
Sagittal
Electrode site
C4
L
R

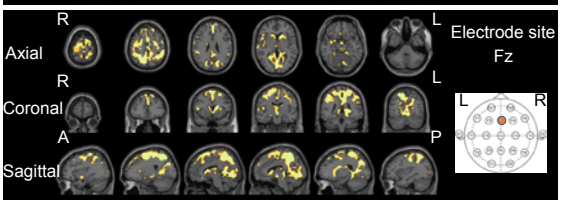
R
L
Axial
R
L
Coronal
A
P
Sagittal
Electrode site
Fz
L
R

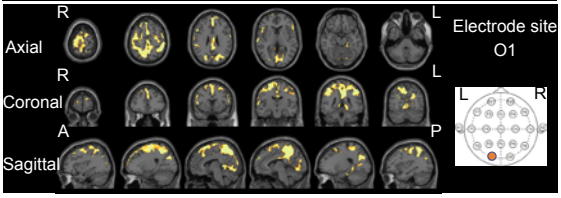
R
L
Axial
R
L
Coronal
A
P
Sagittal
Electrode site
O1
L
R

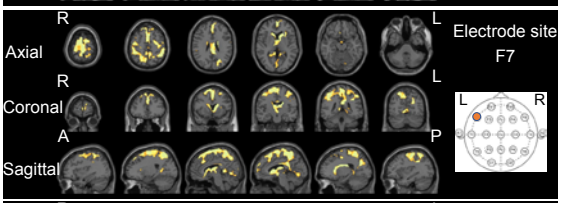
R
L
Axial
R
L
Coronal
A
P
Sagittal
Electrode site
F7
L
R

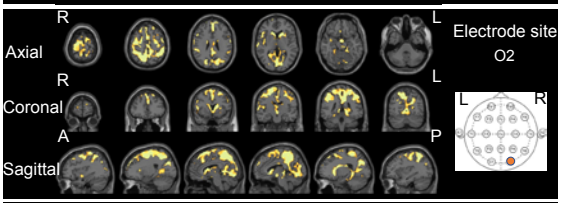
R
L
Axial
R
L
Coronal
A
P
Sagittal
Electrode site
O2
L
R

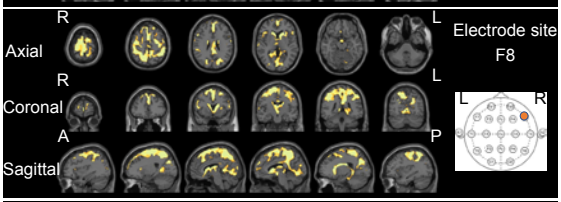
R
L
Axial
R
L
Coronal
A
P
Sagittal
Electrode site
F8
L
R

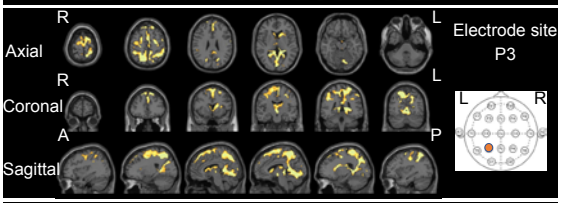
R
L
Axial
R
L
Coronal
A
P
Sagittal
Electrode site
P3
L
R

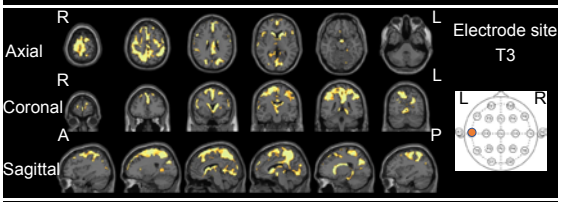
R
L
Axial
R
L
Coronal
A
P
Sagittal
Electrode site
T3
L
R

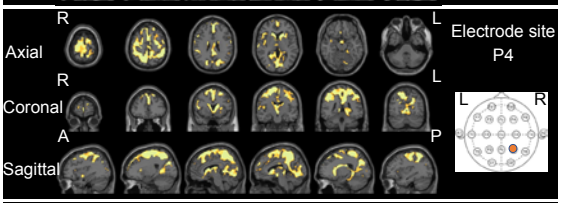
R
L
Axial
R
L
Coronal
A
P
Sagittal
Electrode site
P4
L
R

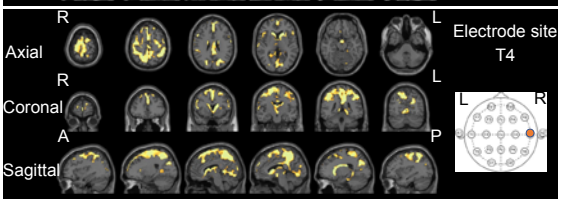
R
L
Axial
R
L
Coronal
A
P
Sagittal
Electrode site
T4
L
R

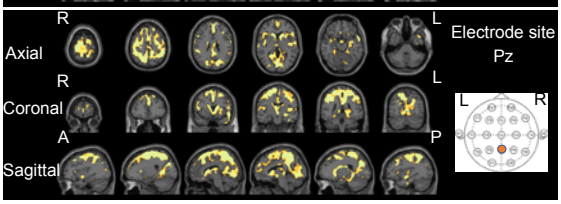
R
L
Axial
R
L
Coronal
A
P
Sagittal
Electrode site
Pz
L
R

Figure S3. Positive AMPAR-theta activity couplings are observed in patients with the focal onset seizures without generalized seizure detected by multiple electrode sites, Related to Figure2

SPM analysis of [^{11}C]K-2 in patients with the focal onset seizures without generalized seizure identifies the brain regions showing a significant positive correlation between $SUVR_{30\text{-}50\ min}$ with white matter as a reference and the amplitude of theta activity in Fp1, Fp2, F3, F4, Fz, F7, F8, C3, C4, T3, T4, T5, T6, P3, P4, Pz, O1,O2 electrode site ($p < 0.05$, $T > 2.35$, one-tailed, FDRc). Scale bar indicates T value of this correlation. R: right side, L: left side, A: anterior side, P: posterior side.

Figure S4

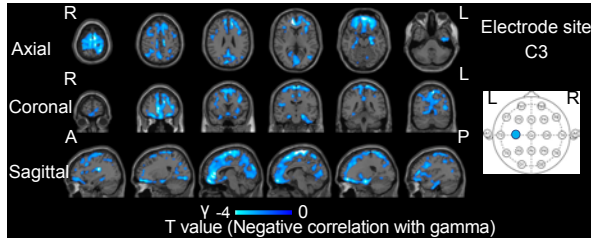
R
L
Axial
Electrode site
C3
R
L
Coronal
L
R
A
P
Sagittal
γ -4
0
T value (Negative correlation with gamma)

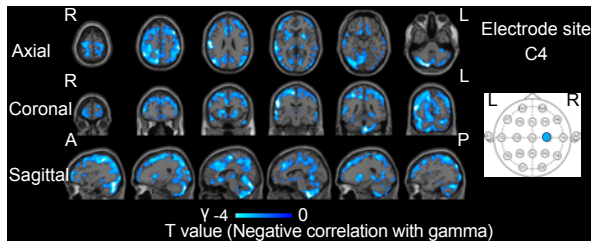
R
L
Axial
Electrode site
C4
R
L
Coronal
L
R
A
P
Sagittal
γ -4
0
T value (Negative correlation with gamma)

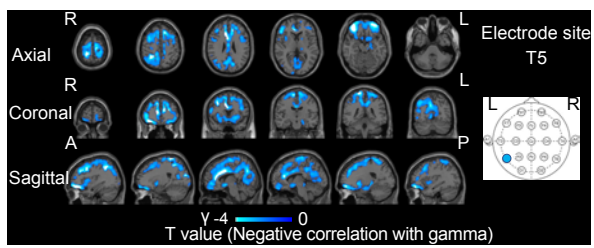
R
L
Axial
Electrode site
T5
R
L
Coronal
L
R
A
P
Sagittal
γ -4
0
T value (Negative correlation with gamma)

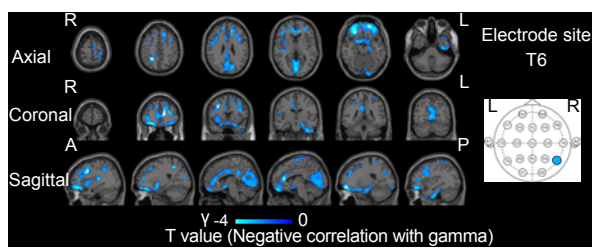
R
L
Axial
Electrode site
T6
R
L
Coronal
L
R
A
P
Sagittal
γ -4
0
T value (Negative correlation with gamma)

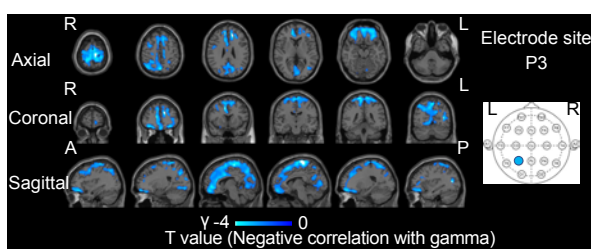
R
L
Axial
Electrode site
P3
R
L
Coronal
L
R
A
P
Sagittal
γ -4
0
T value (Negative correlation with gamma)

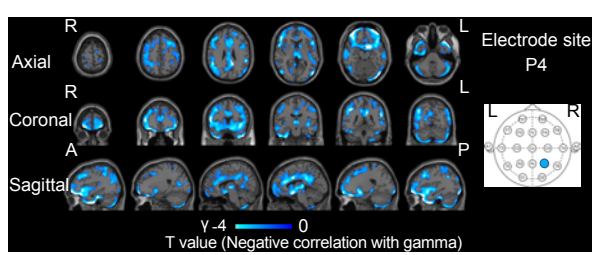
R
L
Axial
Electrode site
P4
R
L
Coronal
L
R
A
P
Sagittal
γ -4
0
T value (Negative correlation with gamma)

Figure S4. Generalized onset seizure downregulates AMPAR levels detected by multiple electrode sites, Related to Figure 4

SPM analysis of [^{11}C]K-2 in patients with the generalized onset seizures identifies the brain regions showing a significant negative correlation between $SUVR_{30\text{-}50\ min}$ with white matter as a reference and the amplitude of gamma activity in C3, C4, T5, T6, P3, P4 electrode sites ($p < 0.05$, $T > 1.94$, one-tailed, FDRc). Scale bar indicates T value of this correlation. R: right side, L: left side, A: anterior side, P: posterior side.